NASA TECHNICAL NOTE

NASA TN D-5863

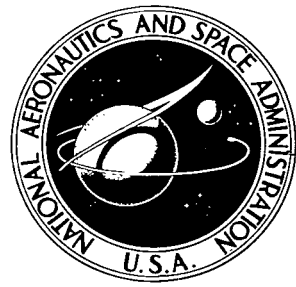

TURBULENT-BOUNDARY-LAYER HEAT-TRANSFER AND TRANSITION MEASUREMENTS WITH SURFACE COOLING AT MACH 6

by Aubrey M. Cary, Jr.

Langley Research Center

Hampton, Va. 23365

NATIONAL AERONAUTICS AND SPACE ADMINISTRATION • WASHINGTON, D. C. • JUNE 1970

1. Report No.	2. Government Accession No.	3. Recipient's Catalog No.
NASA TN D-5863		

4. Title and Subtitle
TURBULENT-BOUNDARY-LAYER HEAT-TRANSFER AND TRANSITION MEASUREMENTS WITH SURFACE COOLING AT MACH 6

5. Report Date
June 1970

6. Performing Organization Code

7. Author(s)
Aubrey M. Cary, Jr.

8. Performing Organization Report No.
L-6825

9. Performing Organization Name and Address
NASA Langley Research Center
Hampton, Va. 23365

10. Work Unit No.
129-01-20-09

11. Contract or Grant No.

12. Sponsoring Agency Name and Address
National Aeronautics and Space Administration
Washington, D.C. 20546

13. Type of Report and Period Covered
Technical Note

14. Sponsoring Agency Code

15. Supplementary Notes

The material presented herein is based on a thesis entitled "Turbulent Boundary Layer Heat Transfer and Transition Measurements With Extreme Surface Cooling at Mach 6" submitted in partial fulfillment of the requirements for the degree of Master of Aerospace Engineering, University of Virginia, Charlottesville, Virginia, August 1969.

16. Abstract

This experimental investigation shows the effect of wall cooling on turbulent heat-transfer and boundary-layer transition for a sharp-leading-edge flat plate at Mach 6 and Reynolds numbers as high as 10^7 in the Langley 20-inch hypersonic wind tunnel. Decreasing the ratio of wall temperature to total temperature $\left(0.19 \leqq T_w/T_t \leqq 0.7\right)$ had little effect on the turbulent heat-transfer coefficient. The Spalding and Chi method best predicted both the level and trend of the heat-transfer data with wall cooling for the virtual origin located at peak heating and using the modified Kármán Reynolds analogy. The transition Reynolds number increased (30 to 60 percent) when the ratio of wall temperature to total temperature decreased, but no transition reversal occurred.

17. Key Words (Suggested by Author(s))	18. Distribution Statement
Turbulent boundary layer Turbulent heat transfer Boundary-layer transition Hypersonic Surface cooling	Unclassified – Unlimited

19. Security Classif. (of this report)	20. Security Classif. (of this page)	21. No. of Pages	22. Price*
Unclassified	Unclassified	48	$3.00

*For sale by the Clearinghouse for Federal Scientific and Technical Information
Springfield, Virginia 22151

TURBULENT-BOUNDARY-LAYER HEAT-TRANSFER AND TRANSITION MEASUREMENTS WITH SURFACE COOLING AT MACH 6[1]

By Aubrey M. Cary, Jr.
Langley Research Center

SUMMARY

This experimental investigation shows the effect of wall cooling on turbulent heat-transfer and boundary-layer transition for a sharp-leading-edge flat plate at Mach 6 and Reynolds numbers as high as 10^7 in the Langley 20-inch hypersonic wind tunnel. Decreasing the ratio of wall temperature to total temperature $\left(0.19 \leqq T_w/T_t \leqq 0.7\right)$ had little effect on the turbulent heat-transfer coefficient. The Spalding and Chi method best predicted both the level and trend of the heat-transfer data with wall cooling for the virtual origin located at peak heating and using the modified Kármán Reynolds analogy. The transition Reynolds number increased (30 to 60 percent) when the ratio of wall temperature to total temperature decreased, but no transition reversal occurred.

INTRODUCTION

Turbulent boundary layers have been observed over large areas of flight vehicles up to Mach 6 (ref. 1) and may be expected at even higher Mach numbers on proposed large vehicles. Since the structural and thermodynamic design of such vehicles will depend upon knowledge of the surface heating and friction, prediction methods that allow an accurate description of laminar, transitional, and turbulent boundary-layer flow are required.

Because of the difficulties inherent in any theoretical approach to calculate the turbulent boundary layer, numerous semiempirical methods for predicting turbulent boundary-layer characteristics have evolved. In several recent attempts (for example, refs. 2, 3, and 4) to establish the validity of available theories and methods for turbulent flow by comparing predictions with experimental skin-friction and heat-transfer data, certain semiempirical methods were found to be superior. Semiempirical methods most commonly found in the literature are the reference temperature (or enthalpy) methods (refs. 5 to 7),

[1]The material presented herein is based on a thesis entitled "Turbulent Boundary Layer Heat Transfer and Transition Measurements With Extreme Surface Cooling at Mach 6" submitted in partial fulfillment of the requirements for the degree of Master of Aerospace Engineering, University of Virginia, Charlottesville, Virginia, August 1969.

the Winkler and Cha method (ref. 8), and the recent methods of references 2 and 9. Available experimental data guided the formulation of each of these methods.

Since most hypersonic flight vehicles will have low wall temperatures in comparison with the total temperature of the flow, prediction methods for turbulent flow must be valid in the low range of the ratio of wall temperature to total temperature $\left(T_w/T_t\right)$. Studies by Spalding and Chi (ref. 2) and Bertram and Neal (ref. 4) have shown a paucity of experimental data for flat-plate turbulent flow with ratios of wall temperature to total temperature below 0.5. In addition, reference 4 showed that predictions of hypersonic turbulent heat transfer from various popular methods could be divergent at low values of T_w/T_t depending on the Mach number range. Consequently, accurate experimental data for the turbulent boundary layer with low ratios of wall temperature to total temperature are needed to determine the most acceptable prediction method for design purposes. The investigations of Bertram and Neal (ref. 4) and Wallace (ref. 10) give some data with low T_w/T_t for comparison purposes, but more extensive and accurate data are necessary in order to establish reliability of a prediction method.

Another perplexing problem area related to the problem of turbulent flow is the prediction of boundary-layer transition. One of the most controversial facets of high-speed boundary-layer transition research has been the effect of heat transfer on the transition Reynolds number. Various results show that heat transfer has no effect on transition Reynolds number (refs. 11 and 12), has a fairly strong effect on transition Reynolds number (refs. 13 and 14), and has even caused a transition reversal (refs. 15 and 16). There have been numerous explanations, although without adequate substantiation, for the conflicting experimental results.

The present investigation proposes to provide additional information on two-dimensional, zero-pressure-gradient turbulent-boundary-layer heat transfer and transition over a wide range of ratios of wall temperature to total temperature and to determine which of the theories presently considered most reliable best predicts the variation of surface heat transfer with wall cooling. Internally cooling a flat-plate model provided wall temperature ratios over the range $0.19 \leqq T_w/T_t \leqq 0.7$. Data were obtained for two unit Reynolds numbers with the stagnation temperature held constant at approximately 533° K and for two angles of attack giving local Mach numbers of 6.0 and 4.9. In all cases laminar flow occurred near the leading edge, but transition always ended before the midpoint of the plate.

SYMBOLS

C_f skin friction coefficient

C_w specific heat of model material

c_p	specific heat of air at constant pressure
M	Mach number
N_{St}	Stanton number, $\frac{\dot{q}}{\rho u c_p (T_{aw} - T_w)}$
p	absolute pressure
$\dot{q}$	surface heat-transfer rate
R	unit Reynolds number, $\frac{\rho u}{\mu}$
R_{crit}	minimum critical Reynolds number
$R_{t,\Delta x}$	transition-length Reynolds number, $\frac{\rho_e u_e \Delta x}{\mu_e}$
$R_{t,infl}$	local Reynolds number based on distance from leading edge to inflection point (see fig. 11)
r	recovery factor
T	temperature
T'	reference temperature
t	time
u	velocity
x	longitudinal distance from plate leading edge
Δx	longitudinal extent of transition region
y	spanwise distance from plate center line
α	angle of attack
γ	ratio of specific heats for air
λ	skin thickness

μ	viscosity
ρ	density

Subscripts:

aw	adiabatic wall
b	based on distance from leading edge to beginning of transition (fig. 11)
e	local conditions at edge of boundary layer
i	local incompressible
t	stagnation
tr	based on distance from leading edge to end of transition (fig. 11)
v	based on distance from virtual origin
w	wall
x	based on distance from leading edge
∞	undisturbed free stream

APPARATUS AND TESTS

Tunnel

Tests were conducted in the Langley 20-inch hypersonic tunnel. This tunnel has a fixed nozzle block and a rectangular test section and is of the blowdown type exhausting to the atmosphere through a movable second minimum. An annular ejector downstream of the test section insures lower starting and running pressures. Normal operating stagnation pressure can be as high as 37 atmospheres, and by using electrical heaters, the stagnation temperature can be as high as 589° K. Test times as long as one-half hour are possible. A calibration of the test core indicates that for the present test conditions, the Mach number is 6.02 ± 0.02. The water concentration in the tunnel airflow was measured to be 1 to 2 parts per million.

A model injection system using a pneumatic cylinder was located on top of the tunnel directly above the test section. A rectangular opening (approximately 55.88 cm by 36.8 cm) allowed the model to be injected to the center line of the test section after the tunnel flow had been established.

Model and Instrumentation

The flat-plate configuration used in this investigation was intended to produce a two-dimensional, zero-pressure-gradient boundary layer along the test surface. The construction and dimensions of the model are shown in figure 1 along with the orientation of the instrumentation. The plate was constructed of AISI 405 stainless steel with the leading-edge thickness measured as 0.0038 ± 0.0008 cm across the span. Coolant passages were located on each side of the model center line as shown in figure 1. For the present tests liquid nitrogen was injected under pressure into one passage on each side of the model center line and allowed to exhaust from the others. The model was mounted to the injection carriage with a strut attached to the model on the side opposite the instrumented surface. (See fig. 1.)

A 2.54-cm-wide cavity was milled into the back of the model until the metal skin between the bottom of the cavity and the flat surface was 0.076 ± 0.0025 cm thick. Thirty-gage iron-constantan thermocouples were then spotwelded to the undersurface of the thin skin along the center line of the model; see table I for the x- and y-locations of the thermocouples. The skin thickness was measured at each thermocouple location for use in the data reduction. The cavity was then filled with a foamed plastic substance with a very low thermal conductivity ($k \approx 0.021$ watt/meter-^{o}K). A stainless-steel cover plate which faired the cavity into the bottom of the plate was then applied.

Pressure orifices were located along a line 3.81 cm from the model center line at the x-locations shown in table I. The orifices were made from standard 0.23 cm outside diameter monel tubing, the end of which was mounted flush with the flat surface of the plate. The pressure and thermocouple leads were run along the base of the strut and out of the test section. The pressure leads were connected to 0 to 6.9×10^3 N/m^2 diaphragm-type electrical transducers (Statham gages).

End plates were applied to the model in both the up and down positions as shown in figure 2. The leading-edge bevel angle of the end plates was 15^{o} and the edge thicknesses facing the flow were approximately 0.005 cm. The end plates were designed to enclose the leading-edge shock at all angles of attack.

Test Conditions and Procedures

Most of the heat-transfer and pressure tests were made with conditions which would give the largest extent of turbulent-boundary-layer flow over the model. Most of the data

were obtained with a stagnation pressure of approximately 3.55×10^6 N/m^2 at a stagnation temperature of approximately 533° K corresponding to a free-stream unit Reynolds number of approximately 2.64×10^5 per cm. Selected heat-transfer tests were performed at an angle of attack of 0° with a stagnation pressure of approximately 1.83×10^6 N/m^2 and a stagnation temperature of approximately 533° K; the corresponding free-stream Reynolds number was approximately 1.46×10^5 per cm.

For the tests at an angle of attack of 8.1° (compression), the stagnation pressure and temperature were 3.55×10^6 N/m^2 and 533° K, respectively. These conditions resulted in a local unit Reynolds number of approximately 3.82×10^5 per cm and a local Mach number of 4.9; the local Reynolds number and Mach number were calculated by use of oblique shock relations, the solutions for which are tabulated in reference 17.

The model was cooled by injecting liquid nitrogen through the coolant passages shown in figure 1. Since the test facility was not airtight, it was necessary to cover the model during the cooling process to prevent frost formation on the instrumented surface. The model, positioned in the injection housing, was covered with aluminum foil and then a rubber sheet connected to each side of the injection housing. When the model had been cooled to the desired temperature, the tunnel was started, and the model was injected into the established stream. As the model plunged from the cavity toward the stream, the rubber sheet was broken and the aluminum foil was ripped away from the model by the tunnel air and dissipated downstream. An observer watched the injection for each run to insure that no aluminum foil or surface frost was present when the model reached the center line of the tunnel test core. The model moved from the sheltered cavity to the tunnel center line in approximately 0.25 second.

The following nominal conditions were used in calculating parameters from all methods:

$\alpha = 0^\circ$	$M_e = M_\infty = 6.0$ $T_{t,e} = T_{t,\infty} = 533^\circ$ K $T_e = T_\infty = 65^\circ$ K
$\alpha = 8.1^\circ$	$M_e = 4.9$ $T_{t,e} = 533^\circ$ K $T_e = 92.2^\circ$ K

The model wall temperature was variable from run to run. Typical surface temperature distributions at $t = 0$ are presented in figure 3. The wall temperature generally varies less than $\pm 15^\circ$ about a mean value; this mean value has been used for the calculations.

DATA REDUCTION

All the experimental data were reduced by use of a nominal free-stream Mach number of 6.0 and measured values of free-stream stagnation pressure and temperature.

Pressure Data

The electrical outputs from the pressure transducers were recorded on a high-speed digital readout recorder about 5 seconds after the model was in final position in the test section of the tunnel. From the calibration data for each transducer, electrical outputs were converted to pressure readings on a card-programed computer. The accuracy of the transducers was 0.25 percent of full-scale pressure.

Heat-Transfer Data

The electrical outputs from the thermocouples were recorded on a high-speed digital readout recorder. The signal from each thermocouple was sampled 20 times each second, converted to a binary digital system, and recorded on magnetic tape. When the model was first positioned at the center line of the tunnel test section, 1 second of the temperature-time data was fitted by the method of least squares to a second-degree polynomial of the form

$$T_w = a + bt + ct^2 \tag{1}$$

where a, b, and c are constants. The time derivative of temperature used to calculate the heating coefficients was computed at the first point of the curve fit. (The derivative was constant for at least the first five points.)

The model wall temperature at the start of the tests varied from approximately 100° K to 341° K. Because of the quick insertion into the test flow (approximately 0.25 sec), the model was considered to have been subjected to a step function in aerodynamic convective heat input. In the absence of radiative and conductive heating, the local surface heating rate for the model was expressed as

$$\dot{q} = C_w \rho_w \lambda \frac{dT_w}{dt} \tag{2}$$

where the model density ρ_w was 7700 kg/m^2. The specific heat of the model material C_w is shown in figure 4 as a function of temperature. These measurements of C_w were made by the National Bureau of Standards with a test specimen from the present model and are accurate to within 0.3 percent for T_w less than 100° K and 0.1 percent for T_w greater than 100° K. The skin thickness λ was measured at each thermocouple location and was 0.076 ± 0.0025 cm.

Radiative heating for the most extreme conditions encountered in this investigation (tunnel wall temperature $\approx 333^{\circ}$ K, model wall temperature $\approx 100^{\circ}$ K) was calculated to be less than 0.50 percent of the aerodynamic heating and thus was neglected for all data. Conduction heating was calculated by use of the three-point finite-difference method described in reference 18. Because spanwise and chordwise conduction heating was calculated to be generally less than 1 percent of the convection heating, no corrections for conduction were applied to the experimental data. The heat conducted to the insulating material backing the instrumented surface was calculated to be less than 1 percent of the convective heat input and was therefore neglected.

The Stanton number was calculated from the relations:

$$N_{St,\infty} = \frac{\dot{q}}{\rho_{\infty} u_{\infty} c_p (T_{aw} - T_w)} \tag{3}$$

or

$$N_{St,e} = \frac{\dot{q}}{\rho_e u_e c_p (T_{aw} - T_w)} \tag{4}$$

where

$$T_{aw} = T_e \left(1 + r \frac{\gamma - 1}{2} M_e^2\right) \tag{5}$$

The recovery factor r was taken to be 0.845 for laminar flow and 0.89 for turbulent flow.

RESULTS AND DISCUSSION

A schlieren photograph of the model without end plates alined at $\alpha = 0^{\circ}$ ($M_{\infty} = 6$) to the free stream is shown in figure 5. The outline of the model and rectangular strut is indicated on the figure. The apparent thickness of the leading-edge shock wave is due to a small roll angle of the model as well as some diffraction. The reflection of the leading-edge shock wave from the tunnel-wall boundary passes the plane of the model well downstream of the rear of the model and thus causes no interference on the instrumented surface.

Selected measurements showing the effects of wall cooling on the local surface pressure distribution were obtained and are shown in figure 6. The scatter in the data occurs because the pressures had not completely "settled out" when the data were recorded. Pressures were recorded approximately 5 seconds after model injection so that the model surface would be at a low and uniform temperature. If the pressures had been allowed to settle, the accuracy would have been better but large temperature gradients would have existed along the plate. When this procedure was used, the pressures were as much as

6 percent higher than the inviscid prediction and there was no trend in the data scatter. By comparing part (a) with part (b) and part (c) with part (d) of figure 6, the data indicate that wall cooling has no obvious effect on the pressure distribution at either angle of attack; however, wall temperature, in the absence of viscous induced effects, should have no effect on the pressure distribution and thus local flow conditions. For all calculations of local flow conditions, the local static pressure was assumed to be the inviscid value.

Extraneous Effects on Heat Transfer

Spanwise and end plate effects.- At two locations on the plate ($x = 29.84$ cm and 36.50 cm), two spanwise thermocouples were located 0.635 cm on each side of a thermocouple on the instrumented center line. For all tests, the end of transition along the center line had occurred before $x = 29$ cm; therefore, the spanwise instrumentation was always located in the turbulent regime. The calculated heating rates for the three spanwise thermocouples at a given x-station generally agreed within 5 percent at an angle of attack of 0° and within 4 percent at an angle of attack of 8.1°. The variation of the heating rates across the short span (1.27 cm) was random, was not affected by wall temperature, and was within the accuracy of the data. Specific data points for the spanwise instrumentation are omitted from all figures in the interest of clarity. In general, the values of spanwise heating for turbulent flow would fall within the bounds of the symbol for the center-line heating at the same x-location.

Effects of end plates on the surface heating (Stanton number) are shown in figure 7 at angles of attack of 0° and 8.1° for a ratio of wall temperature to total temperature of 0.60. A comparison of the heating data for no end plates, end plates up, and end plates down (see fig. 2 for orientation) indicates that the addition of end plates has no appreciable effect on the surface heating along the length of the plate at either angle of attack. The width of the plate was such that disturbances moving from the corner of the leading edge toward the center line of the plate along a Mach line originating at the leading edge would not reach the center line. The data confirm that the heat-transfer distribution down the center portion of the plate was independent of the end plate orientation. The heating data shown in subsequent figures were obtained with the "end plates down" configuration. End plates were used only as a safeguard against extraneous disturbances feeding onto the plate and were used in the down position because the instrumented surface could easily be covered during the cooling process.

Frost formation effects.- The instrumented surface of the plate as well as the leading edge of the model was shielded while the plate was cooled. When the plate was injected, visual checks were made for all tests to insure a frost-free surface during the data-acquisition period. Of approximately 80 runs made during this investigation, slight frost appeared for approximately 20 percent of the runs. Repeat runs, one with slight

surface frost and one with no frost, showed that slight frost had little effect on the surface heating and transition location. An example of the effect of heavy frost formation on the surface heating and transition location is shown in figure 8. Heavy frost on the model surface was present when the plate was cooled while exposed to the atmosphere. The wall temperature distributions for the heavy-frost and no-frost cases are shown to be similar in the upper part of the figure. The heat-transfer distribution with heavy frost (shown by the shaded symbols) shows much data scatter and is at a lower level than the no-frost heating distribution. Heavy frost delays boundary-layer transition as evidenced by the location of peak heating. This increased length to the end of transition might be considered unusual since many investigators have shown that surface roughness usually promotes transition; however, as shown in reference 19, small roughness may delay transition. The sublimation of frost at the model surface may also affect the transition location. In light of the observed effects of frost formation, only data for which the instrumented surface was frost free are presented hereafter.

Effects of Reynolds Number and Wall Cooling on Surface Heating

Typical examples of the surface heat-transfer distributions are shown in figure 9 for an angle of attack of 0° and in figure 10 for an angle of attack of 8.1°. The free-stream Stanton number is plotted against the distance from the leading edge of the plate for various ratios of wall temperature to total temperature. Several runs are plotted for each ratio of wall temperature to total temperature to show the repeatability of the heat-transfer distributions and transition location. Heat-transfer data are repeatable within 10 percent for all cases, and the transition location is repeatable to within 2 cm. Heat-transfer data for representative ratios of wall temperature to total temperature are provided in tables II and III.

At an angle of attack of 0° $\left(R_e/cm = 2.64 \times 10^5\right)$, the laminar heat-transfer data prior to transition are well predicted by the Monaghan T' method (ref. 20). A comparison of parts (a), (b), and (c) of figure 9 shows that the laminar heating is a weak function of the ratio of wall temperature to total temperature for $0.2 \leqq T_w/T_t \leqq 0.6$ as predicted by the T' method. No laminar data are presented for an angle of attack of 8.1° (fig. 10) since transition occurred before the first thermocouple in every case. Five runs were made at an angle of attack of 0° and $R_e/cm = 1.46 \times 10^5$ which are not presented in figure 9. The laminar data for these runs were also predicted well by Monaghan's T' method.

The virtual origin of the turbulent boundary layer was chosen as the location of peak heating near the end of transition (as in ref. 4) and the Reynolds number based on this origin $\left(R_{e,v}\right)$ is illustrated in figure 11. The variation of the turbulent heat transfer with turbulent Reynolds number $\left(R_{e,v}\right)$ based on the distance from the virtual origin is

presented in figure 12 for $M_e = 6.0$ and in figure 13 for $M_e = 4.9$. The heating data are presented as the ratio $N_{St,e}/N_{St,i}$ where the incompressible Stanton number[2] was obtained from reference 21 at the same Reynolds number as $N_{St,e}$. Generally, several runs are presented for each ratio of wall temperature to total temperature including some data for $R_e/cm = 1.46 \times 10^5$. At the lowest ratio of wall temperature to total temperature for both $M_e = 6.0$ and 4.9, the experimental Stanton number decreases more slowly with Reynolds number than the incompressible Stanton number (shown by the increase of $N_{St,e}/N_{St,i}$ with $R_{e,v}$). As the wall temperature is increased, $N_{St,e}/N_{St,i}$ becomes constant with $R_{e,v}$ until at the higher wall temperatures $N_{St,e}/N_{St,i}$ decreases weakly with Reynolds number. Therefore, the slope of the heat transfer with Reynolds number is a function of the ratio of wall temperature to total temperature. Note that the data for $R_{e,v}$ less than approximately 10^6 generally fall below the data for $R_{e,v}$ greater than 10^6. A similar effect was found in reference 4 for a large body of turbulent heating data.

Also presented in figures 12 and 13 are the predictions for the turbulent heating from three methods: the Monaghan turbulent T' method (ref. 5), the Spalding and Chi method (ref. 2), and the $\rho_r\mu_r$ method (ref. 9). The skin-friction predictions from the T' (using the Kármán and Schoenherr skin-friction equation) and Spalding and Chi methods were converted to heat transfer by using a modification of Kármán's Reynolds analogy as presented in reference 4. At $M_e = 6$ (fig. 12), the method which best predicts the level and trend of the data through the range of ratios of wall temperature to total temperature is the Spalding and Chi method. The $\rho_r\mu_r$ method consistently underpredicts the level of the data for each ratio of wall temperature to total temperature and does not match the trend of the data with increasing $R_{e,v}$ as well as the Spalding and Chi method. The T' method substantially overpredicts the level of the data at the lower ratios of wall temperature to total temperature; as the ratio of wall temperature to total temperature is increased to 0.6 and above, good agreement exists between the T' prediction and the experimental data. As previously mentioned, comparisons were with data for which $R_{e,v}$ was greater than 10^6. At $M_e = 4.9$ (fig. 13), the data fall between the predictions of the Spalding and Chi and $\rho_r\mu_r$ methods but generally favor the level of the Spalding and Chi method. The T' method again overpredicts the heat transfer at low ratios of wall temperature to total temperature.

To illustrate clearly the effect of wall cooling on turbulent heat transfer, the data are presented as Stanton number ratio as a function of wall cooling for a specific value of $R_{e,v}$ in figure 14 for $M_e = 6$ and in figure 15 for $M_e = 4.9$. Each data point in figures 14 and 15 was obtained from a fairing of $N_{St,e}/N_{St,i}$ against $R_{e,v}$ at the

---

[2] $N_{St,i}$ was obtained by multiplying the skin-friction coefficient from the Kármán-Schoenherr imcompressible equation by Kármán's value of Reynolds analogy at the same Reynolds number as $N_{St,e}$.

particular value of $R_{e,v}$ indicated in figure 14 or 15. In this form the data show that at both Mach numbers the turbulent heat transfer is approximately independent of the wall cooling for the range of ratios of wall temperature to total temperature for this investigation. Predictions by the same methods shown in figures 12 and 13 as well as predictions by the Van Driest method (ref. 22) using a Reynolds analogy factor of 1.16, the Sommer and Short T' method (ref. 7), the Eckert T' method (ref. 6), and the Winkler and Cha method (ref. 8) are included in figures 14 and 15 for comparison with the data. These engineering methods are most commonly used to estimate hypersonic turbulent boundary-layer skin friction and heat transfer. At $M_e = 6$, the prediction from the Spalding and Chi method agrees with both the level and the trend of the data with wall cooling; at Mach 4.9 the Spalding and Chi method predicts the trend with wall cooling but slightly overpredicts the level of the turbulent heating. The $\rho_r \mu_r$ method predicts the trend but underpredicts the magnitude of the data at both Mach 6 and 4.9. Clearly, at both Mach numbers, the Van Driest and T' methods substantially overpredict the heat transfer at the low ratios of wall temperature to total temperature, and the Winkler and Cha method substantially underpredicts the data at the same low ratios of wall temperature to total temperature.

Previous investigations by Bertram and Neal (ref. 4), Wallace (ref. 10), and Nerem and Hopkins (ref. 23) have shown that the Spalding and Chi method best predicts their turbulent skin-friction and heat-transfer results for the lower ratios of wall temperature to total temperature (or enthalpy). The results of Wallace (M_e = 4 to 9) and Nerem and Hopkins (M_e = 2.5 to 3.5) were obtained in shock tunnels where low ratios of wall enthalpy to total enthalpy were achieved on a room-temperature model by elevating the stagnation enthalpy of the stream; in contrast, the model was cooled and the stagnation temperature held constant for the results of this investigation. The resulting comparisons of experimental data with turbulent prediction methods yielded the equivalent result that the Spalding and Chi method best predicted the data.

A recent investigation by Hopkins, et al. (ref. 24) indicated that the methods of Coles (ref. 25) and Van Driest (ref. 22) best predict the turbulent skin-friction data available above Mach 4 or 5 and $T_w/T_{aw} > 0.3$ when the predictions are based on a momentum thickness Reynolds number rather than on a length Reynolds number. Turbulent heat-transfer data were also better predicted by these same methods when a Reynolds analogy factor $\left(2N_{St}/C_f\right)$ of 1.0 was used instead of the extension of Von Kármán's Reynolds analogy as used herein and when the predictions were based on an energy thickness Reynolds number (obtained by integrating the surface heat-transfer distribution) instead of a length Reynolds number. The present turbulent heating data, included in the analysis of reference 24, were well predicted by Coles' and Van Driest's methods and were significantly underpredicted by Spalding and Chi's method when an energy thickness Reynolds number and a Reynolds analogy factor of 1.0 were used.

In reference 24 a Reynolds analogy factor of 1 was experimentally measured for Mach 6.8 and 7.4 $\left(T_w/T_{aw} \approx 0.3\right)$ and was assumed to remain equal to 1.0 at other Mach numbers and ratios of wall temperature to adiabatic wall temperature for comparing data with prediction methods. If a Reynolds analogy factor of 1.0 had been used with the prediction methods presented in this report instead of the modified Kármán Reynolds analogy, the predictions would be reduced by 9 to 17 percent. A compilation of available experimental measurements of Reynolds analogy for compressible, turbulent-boundary-layer flow presented in reference 26 tend to favor Kármán's values, in general, for T_w/T_t greater than 0.4. Predictions are also sensitive to the choice of the virtual origin for the turbulent boundary layer. For the data presented in figure 9, the momentum thickness Reynolds number was obtained as in reference 24 and this momentum thickness Reynolds number extrapolated to zero by using the Spalding and Chi method. By using this new virtual origin (zero-momentum-thickness location), the Spalding and Chi predictions for a given x-station ($x > 28$ cm) decreased from 7 to 18 percent depending on the Reynolds number and the ratio of wall temperature to total temperature. It thus appears that selecting a "best" method for predicting hypersonic turbulent heating will depend upon the methodology and assumptions involved in the application of the methods (choice of Reynolds analogy factor, virtual origin, and Reynolds number). Data and theory comparisons at very high Reynolds numbers, such as represented by Wallace's results (see presentation of his data in ref. 27), are little affected by at least the choice of virtual origin.

Effects of Wall Cooling on Boundary-Layer Transition

Boundary-layer transition Reynolds numbers were determined from the heat-transfer distributions as indicated in figure 11. The Reynolds number for the beginning of transition was taken as the local unit Reynolds number times the x-distance from the leading edge of the plate to the minimum Stanton number; the Reynolds number for the end of transition was taken as the local unit Reynolds number times the x-distance from the plate leading edge to the location of the maximum Stanton number. (See fig. 11.)

The effect of wall cooling on the transition Reynolds number for the beginning and end of transition at Mach 6 and 4.9 are shown in figure 16 and these data are given in table IV. At Mach 6 transition results are presented for $R_e/cm = 2.65 \times 10^5$ along with limited results for $R_e/cm = 1.46 \times 10^5$. The Mach 6 results for $R_e/cm = 2.65 \times 10^5$ show that the transition Reynolds number increases approximately 40 percent for a decrease in the ratio of wall temperature to adiabatic wall temperature from 0.7 to 0.2. For $R_e/cm = 1.46 \times 10^5$, the transition Reynolds number increases approximately 60 percent for a T_w/T_{aw} decrease from 0.7 to 0.2. The Reynolds number for the beginning and end of transition increase approximately the same percentage through the range of the ratio of wall temperature to adiabatic wall temperature at a given unit Reynolds number.

At Mach 4.9, the Reynolds number for the end of transition increased approximately 30 percent for a T_w/T_{aw} decrease from 0.7 to 0.2. The Reynolds number for the beginning of transition at Mach 4.9 is not shown because transition had begun before the first measuring station for each case.

A comparison of fairings of the present transition data with faired results from previous investigations using sharp-leading-edge (leading-edge thickness $\leqq$ 0.0051 cm) flat plates (refs. 11, 15, 28, 29, and 30) is shown in figure 17 for Mach numbers from 2.4 to 10.2. There appears to be no consistent variation of transition Reynolds number with decreasing ratio of wall temperature to adiabatic wall temperature. Depending upon the investigation, the transition Reynolds number increases, decreases, or first increases and then decreases with decreasing T_w/T_{aw}. The reversal trend for the Mach 8.2 data of Richards and Stollery (ref. 15) was characterized by the transition location moving rearward on the plate with wall cooling until the boundary layer was laminar over the length of the plate; further cooling caused transition to reoccur on the plate and subsequently to move rearward again beyond the end of the plate. This transition-reversal phenomenon has also been observed to occur on cones at lower ratios of wall temperature to adiabatic wall temperature. (See ref. 16.)

Since there is no theoretical approach to explain the effects of variations of flow variables and boundary conditions on compressible boundary-layer transition, experimentally observed transition results have not been satisfactorily correlated. Some insight into the reasons for the differing experimental results may be available from a cursory look at linearized stability theory if one could assume that the variation of the minimum critical Reynolds number (that Reynolds number below which disturbances in the boundary layer will not be amplified) is generally similar to the variation for the transition Reynolds number. This correspondence of R_{crit} and the transition Reynolds number may not exist. Mack's recent solution to the compressible stability equations (ref. 31) has indicated that numerous modes of amplified solutions to the viscous stability equations occur. Solutions prior to Mack's solution were concerned only with the first mode. The numerical results show that wall cooling is stabilizing to the first mode but destabilizes the second and higher modes; also wall cooling increases the value of the frequency which is most unstable in the boundary layer. Thus it appears that depending on the spectrum of disturbances in the boundary layer as well as the Mach number and Reynolds number, wall cooling may or may not produce a stabilizing effect on transition.

If the variation of transition Reynolds number with wall cooling does in fact depend upon the disturbances present in the flow field, it is not surprising that the trends of the experimental results with wall cooling in figure 17 do not agree; each of the sets of data were obtained in different facilities which, in general, have a different disturbance spectrum in the free stream. The complex interrelationships between the various modes of

amplification of disturbances as well as the dependency of boundary-layer stability upon the frequencies of disturbances present combine to form a structure which could in principle allow any variation of transition Reynolds number with wall cooling. The further implication of the theoretical results is that since the flow-field disturbances found in flight would, in general, be different from those found in wind tunnels, the effect of wall cooling on the transition Reynolds number found in wind-tunnel tests may not be representative of the effect found in flight tests. It is highly probable that in order to obtain a meaningful correlation of wind-tunnel transition results, additional parameters such as the spectrum of free-stream disturbances will be needed.

The variation of transition Reynolds number with unit Reynolds number for selected values of the ratio of wall temperature to total temperature is shown for Mach 6 on the left-hand side of figure 18. The transition Reynolds number increases with the local unit Reynolds number to the 0.4 to 0.45 power through the wall temperature range. In contrast, the data of Richards and Stollery (ref. 15) at Mach 8.2 shown on the right-hand side of figure 18 show that the transition Reynolds number increases much more rapidly with unit Reynolds number as the ratio of wall temperature to total temperature is decreased. There are many references available which analyze the effect of unit Reynolds number on the transition Reynolds number for supersonic and hypersonic speeds (see, for example, ref. 32), but these analyses are only for moderate values of the ratio of wall temperature to total temperature. Generally, previous investigators found the unit Reynolds number effect to be similar to the results for the present investigation.

Information concerning the effect of wall cooling on the extent of the transition region is available from the data at Mach 6. Potter and Whitfield (ref. 32) have shown for adiabatic wall and near-adiabatic wall conditions that the Reynolds number based on length of the transition region for two-dimensional flow is fairly independent of unit Reynolds number and leading-edge geometry. The correlation which resulted was of the form

$$R_{t,\Delta x} = f\left(M_e, R_{t,infl}\right) \tag{6}$$

where these Reynolds numbers are illustrated in figure 11. This correlation was shown to be independent of sweep angle at Mach 8 in reference 11. The present data are presented according to the Potter and Whitfield correlation in figure 19. The solid lines shown in figure 19 for each Mach number are taken from the Potter and Whitfield correlation. Data from the present investigation representing a variation in the ratio of wall temperature to total temperature from 0.19 to 0.70 are in substantial agreement with the correlated curves. The agreement indicates that at least for Mach 6, the Potter and Whitfield correlation for the length of the transition region is independent of heat transfer as well as unit Reynolds number and leading-edge geometry.

CONCLUSIONS

A study of the effect of wall cooling on zero-pressure-gradient turbulent-boundary-layer heat transfer and laminar-boundary-layer transition has been conducted at a free-stream Mach number of 6 and Reynolds numbers per cm of 2.64×10^5 and 1.46×10^5 in the Langley 20-inch hypersonic tunnel. The wall temperature of a sharp-leading-edge flat plate was varied by internal cooling to yield a range of the ratio of wall temperature to total temperature (T_w/T_t) from 0.19 to 0.70 (with no surface frost) for a total temperature of 533° K. With the model positioned in the tunnel test section at angles of attack of 0° and 8.1°, the local Mach numbers were 6.0 and 4.9, respectively. The conclusions derived from this study are as follows:

(1) Although light frost had little effect on the results, heavy frost formation on the model significantly affected the level of the surface heating as well as the location of boundary-layer transition; therefore only data for frost-free conditions were included in the analysis.

(2) Decreasing the ratio of wall temperature to total temperature $(0.19 \leqq T_w/T_t \leqq 0.7)$ had little effect on the heat-transfer coefficient at either Mach 6 or Mach 4.9.

(3) With the virtual origin chosen as the point of peak heating near the end of transition, the Spalding and Chi method gave a good prediction of the turbulent heat transfer (for a local Reynolds number based on the distance from the virtual origin greater than 10^6) at both Mach 6 and Mach 4.9 over the entire range of the ratio of wall temperature to total temperature. The turbulent T' and Winkler and Cha methods were found to be inadequate for predicting the heating for the low ratios of wall temperature to total temperature. This conclusion is true only when it is assumed that the virtual origin of turbulent flow is at peak heating and that the modified Kármán Reynolds analogy applies.

(4) For a given Mach number and unit Reynolds number, transition Reynolds number increased 30 to 60 percent with decreasing ratio of wall temperature to total temperature, and no transition reversal occurred.

Langley Research Center,
National Aeronautics and Space Administration,
Hampton, Va., April 3, 1970.

REFERENCES

1. Banner, Richard D.; and Kuhl, Albert E.: A Summary of X-15 Heat-Transfer and Skin-Friction Measurements. NASA TM X-1210, 1966.

2. Spalding, D. B.; and Chi, S. W.: The Drag of a Compressible Turbulent Boundary Layer on a Smooth Flat Plate With and Without Heat Transfer. Jour. Fluid Mech., vol. 18, pt. 1, Jan. 1964, pp. 117-143.

3. Peterson, John B., Jr.: A Comparison of Experimental and Theoretical Results for the Compressible Turbulent-Boundary-Layer Skin Friction With Zero Pressure Gradient. NASA TN D-1795, 1963.

4. Bertram, Mitchel H.; and Neal, Luther, Jr.: Recent Experiments in Hypersonic Turbulent Boundary Layers. Presented at the AGARD Specialists' Meeting on Recent Developments in Boundary-Layer Research (Naples, Italy), May 10-14, 1965.

5. Monaghan, R. J.: On the Behaviour of Boundary Layers at Supersonic Speeds. Fifth International Aeronautical Conference, Rita J. Turino and Caroline Taylor, eds., Inst. Aeron. Sci., Inc., June 1955, pp. 277-315.

6. Eckert, E. R. G.: Engineering Relations for Friction and Heat Transfer to Surfaces in High Velocity Flow. J. Aeronaut. Sci. (Readers' Forum), vol. 22, no. 8, Aug. 1955, pp. 585-587.

7. Sommer, Simon C.; and Short, Barbara J.: Free-Flight Measurements of Turbulent-Boundary-Layer Skin Friction in the Presence of Severe Aerodynamic Heating at Mach Numbers From 2.8 to 7.0. NACA TN 3391, 1955.

8. Winkler, Eva M.; and Cha, Moon H.: Investigation of Flat Plate Hypersonic Turbulent Boundary Layers With Heat Transfer at a Mach Number of 5.2. NAVORD Rep. 6631, U.S. Navy, Sept. 15, 1959.

9. Nagel, A. L.; Fitzsimmons, H. D.; and Doyle, L. B.: Analysis of Hypersonic Pressure and Heat Transfer Tests on Delta Wings With Laminar and Turbulent Boundary Layers. NASA CR-535, 1966.

10. Wallace, J. E.: Hypersonic Turbulent Boundary-Layer Studies at Cold Wall Conditions. Proceedings of the 1967 Heat Transfer and Fluid Mechanics Institute, Paul A. Libby, Daniel B. Olfe, and Charles W. Van Atta, eds., Stanford Univ. Press, c.1967, pp. 427-451.

11. Deem, Ralph E.; and Murphy, James S.: Flat Plate Boundary Layer Transition at Hypersonic Speeds. AIAA Pap. No. 65-128, Jan. 1965.

12. Everhart, Philip E.; and Hamilton, H. Harris: Experimental Investigation of Boundary-Layer Transition on a Cooled 7.5° Total-Angle Cone at Mach 10. NASA TN D-4188, 1967.

13. Low, George M.: Boundary-Layer Transition at Supersonic Speeds. NACA RM E56E10, 1956.

14. Braslow, Albert L.: A Review of Factors Affecting Boundary-Layer Transition. NASA TN D-3384, 1966.

15. Richards, B. E.; and Stollery, J. L.: Transition Reversal on a Flat Plate at Hypersonic Speeds. Recent Developments in Boundary Layer Research, Pt. I, AGARDograph 97, May 1965, pp. 477-501.

16. Wisniewski, Richard J.; and Jack, John R.: Recent Studies on the Effect of Cooling on Boundary-Layer Transition at Mach 4. J. Aerospace Sci. (Readers' Forum), vol. 28, no. 3, Mar. 1961, pp. 250-251.

17. Dennard, John S.; and Spencer, Patricia B.: Ideal-Gas Tables for Oblique-Shock Flow Parameters in Air at Mach Numbers From 1.05 to 12.0. NASA TN D-2221, 1964.

18. Bertram, Mitchel H.; and Everhart, Philip E.: An Experimental Study of the Pressure and Heat-Transfer Distribution on a 70° Sweep Slab Delta Wing in Hypersonic Flow. NASA TR R-153, 1963.

19. Holloway, Paul F.; and Sterrett, James R.: Effect of Controlled Surface Roughness on Boundary-Layer Transition and Heat Transfer at Mach Numbers of 4.8 and 6.0. NASA TN D-2054, 1964.

20. Monaghan, R. J.: An Approximate Solution of the Compressible Laminar Boundary Layer on a Flat Plate. R. & M. No. 2760, Brit. A.R.C., 1953.

21. Neal, Luther, Jr.; and Bertram, Mitchel H.: Turbulent-Skin-Friction and Heat-Transfer Charts Adapted From the Spalding and Chi Method. NASA TN D-3969, 1967.

22. Van Driest, E. R.: The Problem of Aerodynamic Heating. Aeronaut. Eng. Rev., vol. 15, no. 10, Oct. 1956, pp. 26-41.

23. Nerem, R. M.; and Hopkins, R. A.: An Experimental Investigation of Heat Transfer From a Highly Cooled Turbulent Boundary Layer. AIAA Pap. No. 68-43, Jan. 1968.

24. Hopkins, Edward J.; Rubesin, Morris W.; Inouye, Mamoru; Keener, Earl R.; Mateer, George C.; and Polek, Thomas E.: Summary and Correlation of Skin-Friction and Heat-Transfer Data for a Hypersonic Turbulent Boundary Layer on Simple Shapes. NASA TN D-5089, 1969.

25. Coles, D. E.: The Turbulent Boundary Layer in a Compressible Fluid. U.S. Air Force Proj., Rand Rep. R-403-PR, RAND Corp., Sept. 1962.

26. Cary, Aubrey M., Jr.: Summary of Available Information on Reynolds Analogy for Zero-Pressure-Gradient, Compressible, Turbulent-Boundary-Layer Flow. NASA TN D-5560, 1970.

27. Bertram, Mitchel H.; Cary, Aubrey M., Jr.; and Whitehead, Allen H., Jr.: Experiments With Hypersonic Turbulent Boundary Layers on Flat Plates and Delta Wings. Hypersonic Boundary Layers and Flow Fields, AGARD CP No. 30, May 1968, pp. 1-1 – 1.21.

28. Higgins, Robert W.; and Pappas, Constantine C.: An Experimental Investigation of the Effect of Surface Heating on Boundary-Layer Transition on a Flat Plate in Supersonic Flow. NACA TN 2351, 1951.

29. Richards, B. E.; and Stollery, J. L.: Further Experiments on Transition Reversal at Hypersonic Speeds. AIAA J., vol. 4, no. 12, Dec. 1966, pp. 2224-2226.

30. Maddalon, Dal V.: Effect of Varying Wall Temperature and Total Temperature on Transition Reynolds Number at Mach 6.8. AIAA J., vol. 7, no. 12, Dec. 1969, pp. 2355-2357.

31. Mack, L. M.: The Stability of the Compressible Laminar Boundary Layer According to a Direct Numerical Solution. Recent Developments in Boundary Layer Research, Pt. I, AGARDograph 97, May 1965, pp. 329-362.

32. Potter, J. Leith; and Whitfield, Jack D.: Effects of Unit Reynolds Number, Nose Bluntness, and Roughness on Boundary Layer Transition. AGARD Rep. 256, Apr. 1960.

TABLE I.- LOCATIONS OF INSTRUMENTATION

[Dimensions are in cm]

Thermocouple	x	y
1	7.30	0
2	9.21	
3	10.16	
4	11.12	
5	13.03	
6	13.97	
7	14.92	
8	15.88	
9	16.84	
10	19.38	
11	21.27	
12	22.22	
13	23.19	
14	24.12	
15	26.99	
16	27.94	
17	28.89	
18	29.84	
19	29.84	0.635
20	29.84	-0.635
21	30.80	0
22	31.74	
23	34.60	
24	35.57	
25	36.50	
26	37.48	
27	37.48	.635
28	37.48	-.635
29	38.41	0
30	39.38	
31	42.22	
32	43.19	
33	44.14	
34	45.10	
35	46.04	
36	47.00	
37	49.20	
38	50.18	

Pressure orifice	x	y
1	7.62	3.81
2	12.70	
3	17.78	
4	35.57	
5	40.00	
6	45.73	
7	50.80	

TABLE II.- HEAT-TRANSFER DATA FOR $M_e = 6.0$

$[M_\infty = 6.0; \quad \alpha = 0^o]$

x, cm	$N_{St,\infty}$
$R_e/cm = 0.31 \times 10^6$;	$T_w/T_t = 0.7$
7.30	2.68×10^4
9.20	4.25
10.16	5.22
11.11	5.91
13.02	8.09
13.97	8.81
14.92	8.61
15.87	8.11
16.84	7.24
19.38	6.82
21.27	6.53
22.22	6.59
23.19	6.47
24.13	5.85
27.94	5.63
28.90	5.86
29.85	5.59
31.75	5.74
34.61	5.61
35.58	5.49
36.51	5.27
37.49	5.04
38.41	5.37
39.38	4.85
42.21	5.13
43.19	4.78
44.13	4.88
45.10	4.60
46.04	4.36
47.00	4.55
49.20	5.06

x, cm	$N_{St,\infty}$
$R_e/cm = 0.26 \times 10^6$;	$T_w/T_t = 0.6$
7.30	2.86×10^4
9.20	2.80
10.16	2.98
11.11	3.41
13.02	5.19
13.97	6.05
14.92	7.56
15.87	8.31
16.84	8.36
19.38	8.11
21.27	7.69
22.22	7.70
23.19	7.45
24.13	6.99
27.94	6.40
28.90	6.44
29.85	6.53
31.75	6.44
34.61	6.36
35.58	6.44
36.51	5.78
37.49	5.82
38.41	5.89
39.38	5.57
42.21	5.88
43.19	5.65
44.13	5.53
45.10	5.61
46.04	5.49
47.00	5.44
49.20	5.84

TABLE II.- HEAT-TRANSFER DATA FOR $M_e = 6.0$ – Continued

x, cm	$N_{St,\infty}$	x, cm	$N_{St,\infty}$
$R_e/cm = 0.26 \times 10^6$; $T_w/T_t = 0.5$		$R_e/cm = 0.27 \times 10^6$; $T_w/T_t = 0.4$	
7.30	2.98×10^4	7.30	2.95×10^4
9.20	3.12	9.20	2.98
10.16	3.25	10.16	2.83
11.11	3.91	11.11	3.03
13.02	4.65	13.02	3.13
13.97	6.56	13.97	4.67
14.92	7.69	14.92	6.01
15.87	8.69	15.87	7.19
16.84	8.54	16.84	7.65
19.38	8.54	19.38	8.54
21.27	7.95	21.27	7.71
22.22	7.92	22.22	7.72
23.19	7.51	23.19	7.57
24.13	7.21	24.13	6.86
27.94	6.67	27.94	6.77
28.90	6.82	28.90	6.26
29.85	6.75	29.85	6.59
31.75	6.95	31.75	6.25
34.61	6.46	34.61	6.13
35.58	6.30	35.58	6.40
36.51	6.16	36.51	5.98
37.49	6.02	37.49	5.63
38.41	6.14	38.41	5.64
39.38	5.89	39.38	5.17
42.41	5.94	42.21	5.63
43.19	5.58	43.19	5.35
44.13	5.57	44.13	5.43
45.10	5.64	45.10	5.25
46.04	5.46	46.04	5.02
47.00	5.42	47.00	4.94
49.20	5.40	49.20	4.79

TABLE II.- HEAT-TRANSFER DATA FOR $M_e = 6.0$ – Continued

x, cm	$N_{St,\infty}$
$R_e/cm = 0.27 \times 10^6$; $T_w/T_t = 0.3$	
7.30	3.03×10^4
9.20	2.88
10.16	2.80
11.11	2.80
13.02	2.87
13.97	3.80
14.92	4.53
15.87	5.88
16.84	6.76
19.38	9.05
21.27	8.99
22.22	9.18
23.19	8.82
24.13	8.21
27.94	7.06
28.90	7.01
29.85	6.92
31.75	6.89
34.61	6.62
35.58	6.53
36.51	6.17
37.49	6.06
38.41	6.24
39.38	5.74
42.21	5.66
43.19	5.20
44.13	5.53
45.10	5.78
46.04	5.33
47.00	5.19
49.20	4.86

x, cm	$N_{St,\infty}$
$R_e/cm = 0.27 \times 10^6$; $T_w/T_t = 0.2$	
7.30	2.95×10^4
9.20	2.82
10.16	2.64
11.11	2.64
13.02	2.53
13.97	3.36
14.92	3.95
15.87	4.72
16.84	5.28
19.38	8.64
21.27	9.30
22.22	9.45
23.19	9.15
24.13	8.70
27.94	8.23
28.90	8.09
29.85	7.84
31.75	8.15
34.61	7.71
35.58	7.99
36.51	7.40
37.49	7.13
38.41	6.74
39.38	6.53
42.21	6.41
43.19	6.17
44.13	6.13
45.10	6.15
46.04	5.62
47.00	5.81
49.20	6.00

TABLE II.- HEAT-TRANSFER DATA FOR $M_e = 6.0$ – Continued

x, cm	$N_{St,\infty}$
$R_e/cm = 0.14 \times 10^6$; $T_w/T_t = 0.6$	
7.30	3.65×10^4
9.20	3.69
10.16	3.62
11.11	3.53
13.02	3.91
13.97	4.28
14.92	4.73
15.87	5.45
16.84	5.83
19.38	7.81
21.27	9.04
22.22	9.66
23.19	9.23
24.13	8.91
27.94	8.02
28.90	7.95
29.85	7.78
31.75	8.03
34.61	7.40
35.58	7.88
36.51	6.84
37.49	6.72
38.41	6.86
39.38	6.64
42.21	6.92
43.19	6.74
44.13	6.12
45.10	6.22
46.04	5.99
47.00	6.13
49.20	6.62

x, cm	$N_{St,\infty}$
$R_e/cm = 0.14 \times 10^6$; $T_w/T_t = 0.4$	
7.30	3.65×10^4
9.20	3.20
10.16	2.78
11.11	3.07
13.02	3.42
13.97	3.95
14.92	4.30
15.87	4.47
16.84	4.63
19.38	5.77
21.27	7.09
22.22	8.10
23.19	8.45
24.13	8.51
27.94	8.42
28.90	8.37
29.85	8.27
31.75	7.82
34.61	7.23
35.58	7.92
36.51	6.86
37.49	7.05
38.41	7.27
39.38	6.53
42.21	6.63
43.19	6.49
44.13	6.47
45.10	6.56
46.04	6.16
47.00	6.03
49.20	6.15

TABLE II.- HEAT-TRANSFER DATA FOR $M_e = 6.0$ – Concluded

x, cm	$N_{St,\infty}$
$R_e/cm = 0.14 \times 10^6$; $T_w/T_t = 0.2$	
7.30	3.30×10^4
9.20	3.78
10.16	3.33
11.11	3.02
13.02	2.91
13.97	2.79
14.92	2.65
15.87	2.79
16.84	---
19.38	2.89
21.27	3.94
22.22	4.30
23.19	4.63
24.13	4.73
27.94	7.72
28.90	8.23
29.85	8.73
31.75	8.75
34.61	9.15
35.58	8.92
36.51	8.40
37.49	8.14
38.41	8.06
39.38	---
42.41	7.58
43.19	7.21
44.13	7.43
45.10	7.56
46.04	7.58
47.00	7.18
49.20	8.12

TABLE III.- HEAT-TRANSFER DATA FOR $M_e = 4.9$

$[M_\infty = 6.0; \quad \alpha = 8.1^\circ]$

x, cm	$N_{St,\infty}$	x, cm	$N_{St,\infty}$
$R_e/cm = 0.39 \times 10^6$; $T_w/T_t = 0.6$		$R_e/cm = 0.39 \times 10^6$; $T_w/T_t = 0.4$	
7.30	10.82×10^4	7.30	8.93×10^4
9.20	17.67	9.20	13.74
10.16	19.55	10.16	16.13
11.11	18.18	11.11	17.25
13.02	17.41	13.02	17.43
13.97	17.23	13.97	17.64
14.92	16.63	14.92	17.11
15.87	16.38	15.87	16.80
16.84	14.82	16.84	14.91
19.38	14.57	19.38	15.20
21.27	14.29	21.27	14.58
22.22	14.70	22.22	14.95
23.19	14.04	23.19	14.60
24.13	13.47	24.13	13.85
27.94	12.93	27.94	13.42
28.90	12.85	28.90	13.57
29.85	13.10	29.85	13.77
31.75	12.97	31.75	13.82
34.61	12.70	34.61	13.36
35.58	13.03	35.58	13.64
36.51	12.15	36.51	12.88
37.49	12.34	37.49	12.76
38.41	12.11	38.41	12.79
39.38	11.95	39.38	12.33
42.21	11.91	42.21	12.32
43.19	11.73	43.19	11.98
44.13	11.65	44.13	11.89
45.10	11.72	45.10	12.10
46.04	11.36	46.04	11.84
47.00	10.98	47.00	11.76
49.20	11.59	49.20	12.08

TABLE III.- HEAT-TRANSFER DATA FOR $M_e = 4.9$ – Concluded

x, cm	$N_{St,\infty}$
$R_e/cm = 0.38 \times 10^6$; $T_w/T_t = 0.3$	
7.30	7.79×10^4
9.20	11.52
10.16	16.05
11.11	18.52
13.02	18.46
13.97	19.00
14.92	18.37
15.87	17.95
16.84	15.83
19.38	16.06
21.27	15.55
22.22	15.95
23.19	15.49
24.13	14.70
27.94	14.04
28.90	14.17
29.85	14.24
31.75	14.44
34.61	14.36
35.58	14.65
36.51	13.71
37.49	14.01
38.41	14.01
39.38	13.67
42.41	13.81
43.19	13.55
44.13	13.51
45.10	13.48
46.04	12.85
47.00	12.05
49.20	12.50

x, cm	$N_{St,\infty}$
$R_e/cm = 0.37 \times 10^6$; $T_w/T_t = 0.25$	
7.30	8.06×10^4
9.20	11.46
10.16	14.70
11.11	17.77
13.02	18.09
13.97	19.15
14.92	18.65
15.87	18.09
16.84	15.45
19.38	16.05
21.27	15.20
22.22	15.64
23.19	15.09
24.13	14.28
27.94	14.09
28.90	14.35
29.85	14.45
31.75	14.80
34.61	14.73
35.58	14.92
36.51	14.06
37.49	14.20
38.41	14.13
39.38	13.52
42.21	13.78
43.19	13.54
44.13	13.54
45.10	13.78
46.04	13.44
47.00	13.14
49.20	13.70

TABLE IV.- TRANSITION DATA

T_w/T_t	R_e/cm	x_b, cm	x_{tr}, cm
M_e = 6.0			
0.190	2.69×10^5	12.70	21.59
.190	2.72	11.68	21.09
.215	2.69	12.20	20.32
.240	2.60	12.70	18.80
.290	2.72	12.20	18.80
.310	2.69	10.92	16.77
.340	2.70	9.90	17.78
.360	2.70	10.41	16.36
.380	2.61	10.92	16.51
.395	2.70	10.16	17.12
.420	2.70	10.41	17.15
.420	2.68	11.17	15.89
.450	2.67	10.67	14.74
.460	2.66	10.41	14.74
.480	2.58	9.40	16.13
.520	2.70	9.91	15.37
.565	2.61	9.14	14.49
.575	2.61	10.15	16.51
.580	2.74	9.40	14.61

T_w/T_t	R_e/cm	x_b, cm	x_{tr}, cm
M_e = 6.0			
0.580	2.64×10^5	9.90	16.76
.600	2.70	9.90	14.61
.700	3.08	8.13	13.46
.190	1.39	18.04	30.60
.400	1.44	13.47	23.62
.550	1.46	13.97	21.47
.580	1.35	13.22	21.34
.600	1.43	11.69	19.82
M_e = 4.9			
0.25	3.70×10^5	<7.30	11.69
.26	3.88	↓	11.18
.32	3.79	↓	11.31
.38	3.65	↓	10.67
.44	3.62	↓	10.42
.51	3.82	↓	10.16
.59	3.76	↓	10.16
.60	3.78	↓	9.65
.66	3.88	↓	9.52

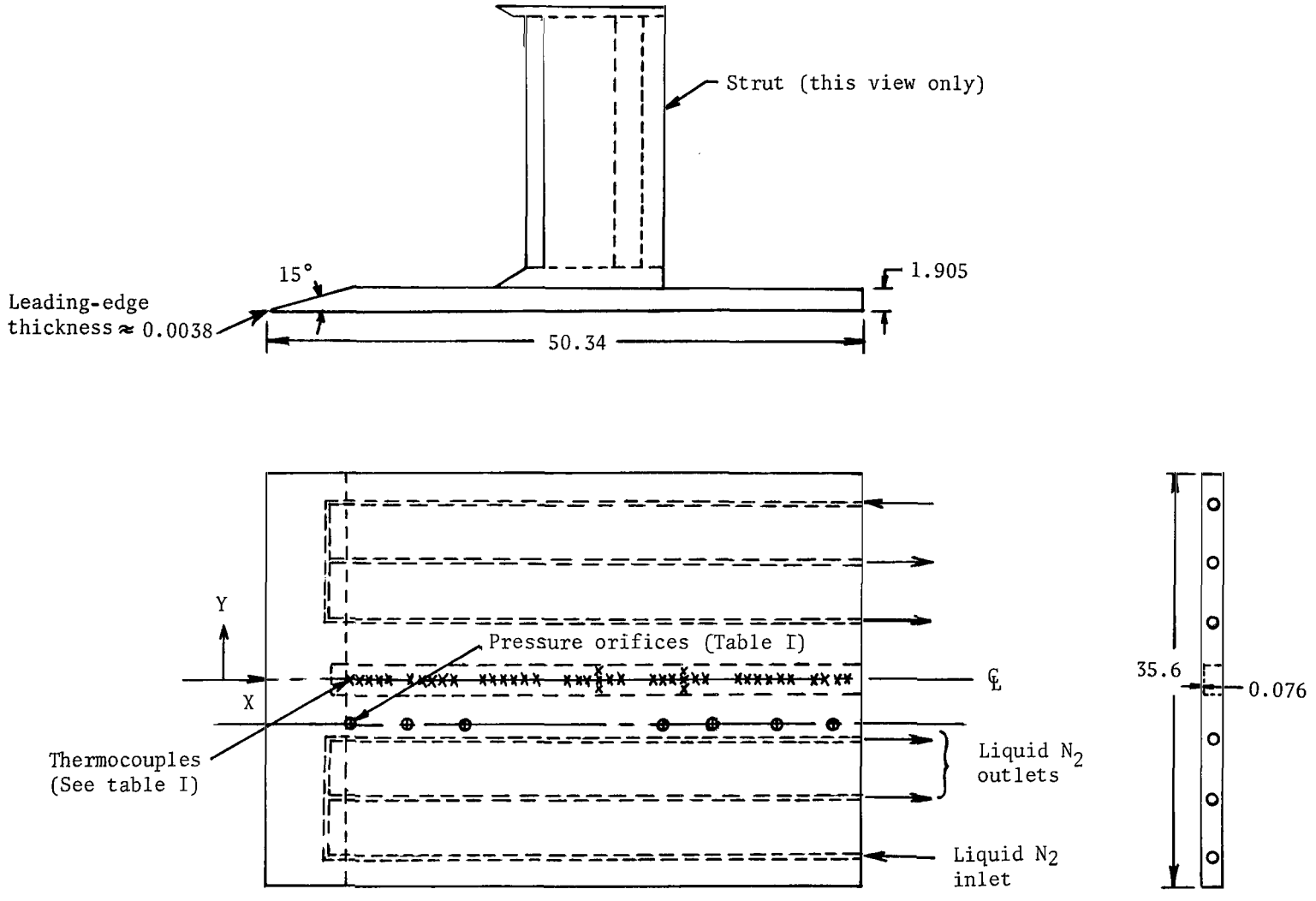

Figure 1.- Model dimensions and instrumentation. (All dimensions are in cm.)

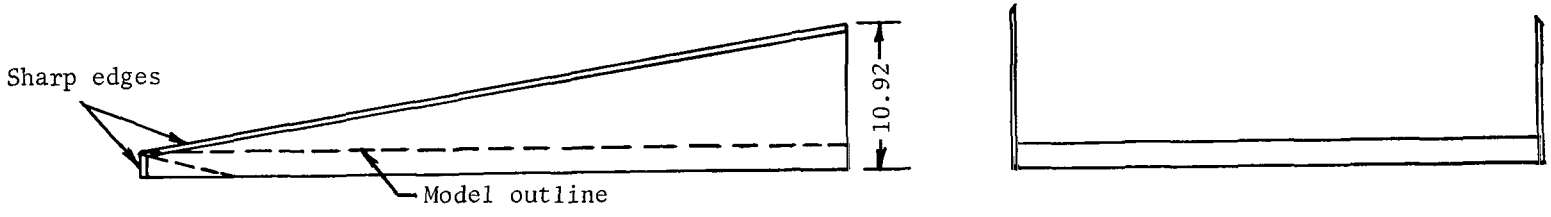

(a) End plates up.

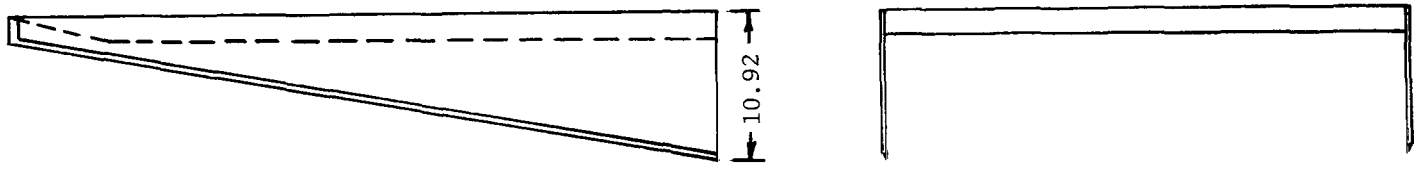

(b) End plates down.

Figure 2.- Orientation of end plates. (All dimensions are in cm.)

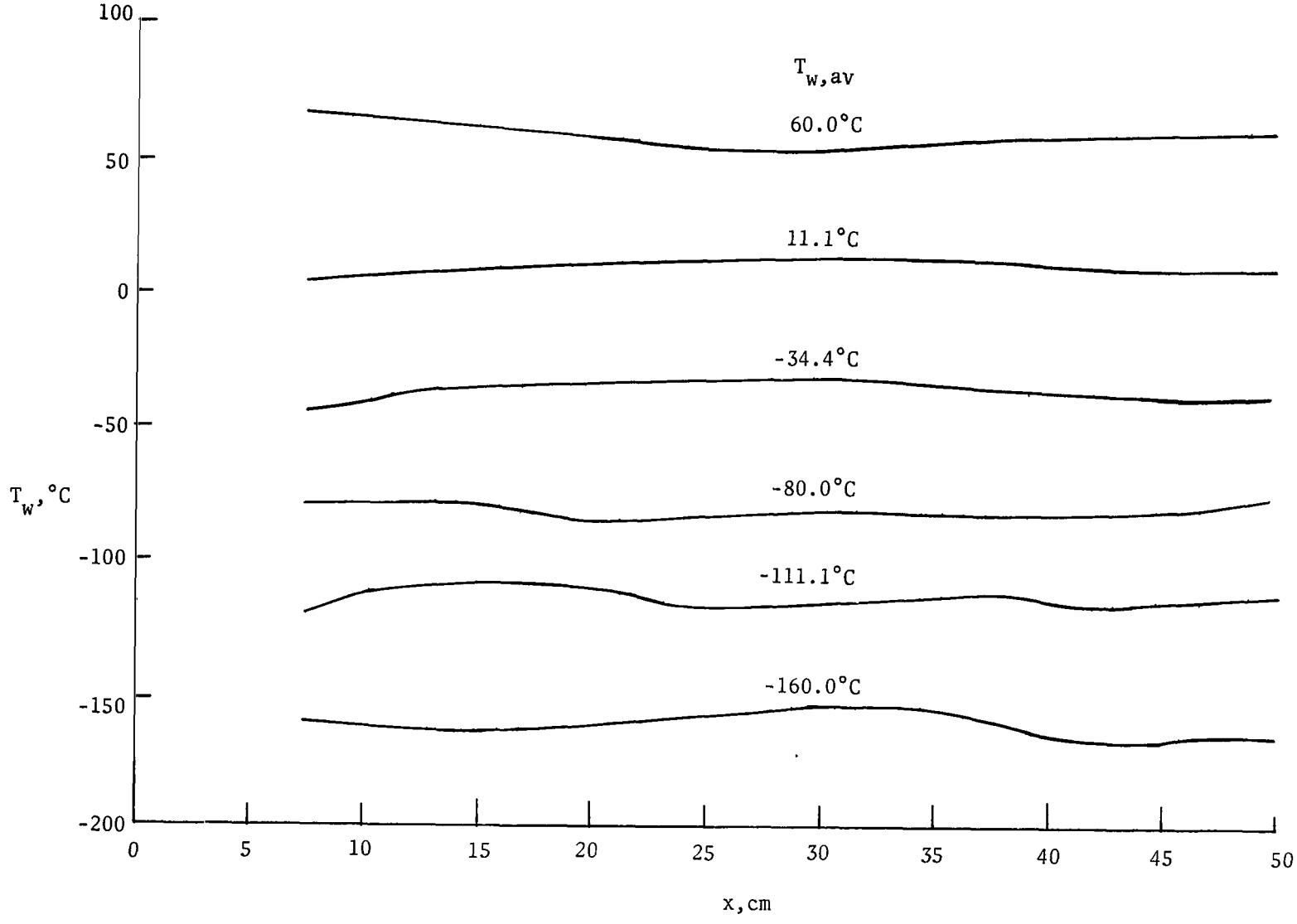

Figure 3.- Typical surface temperature distributions at the onset of testing.

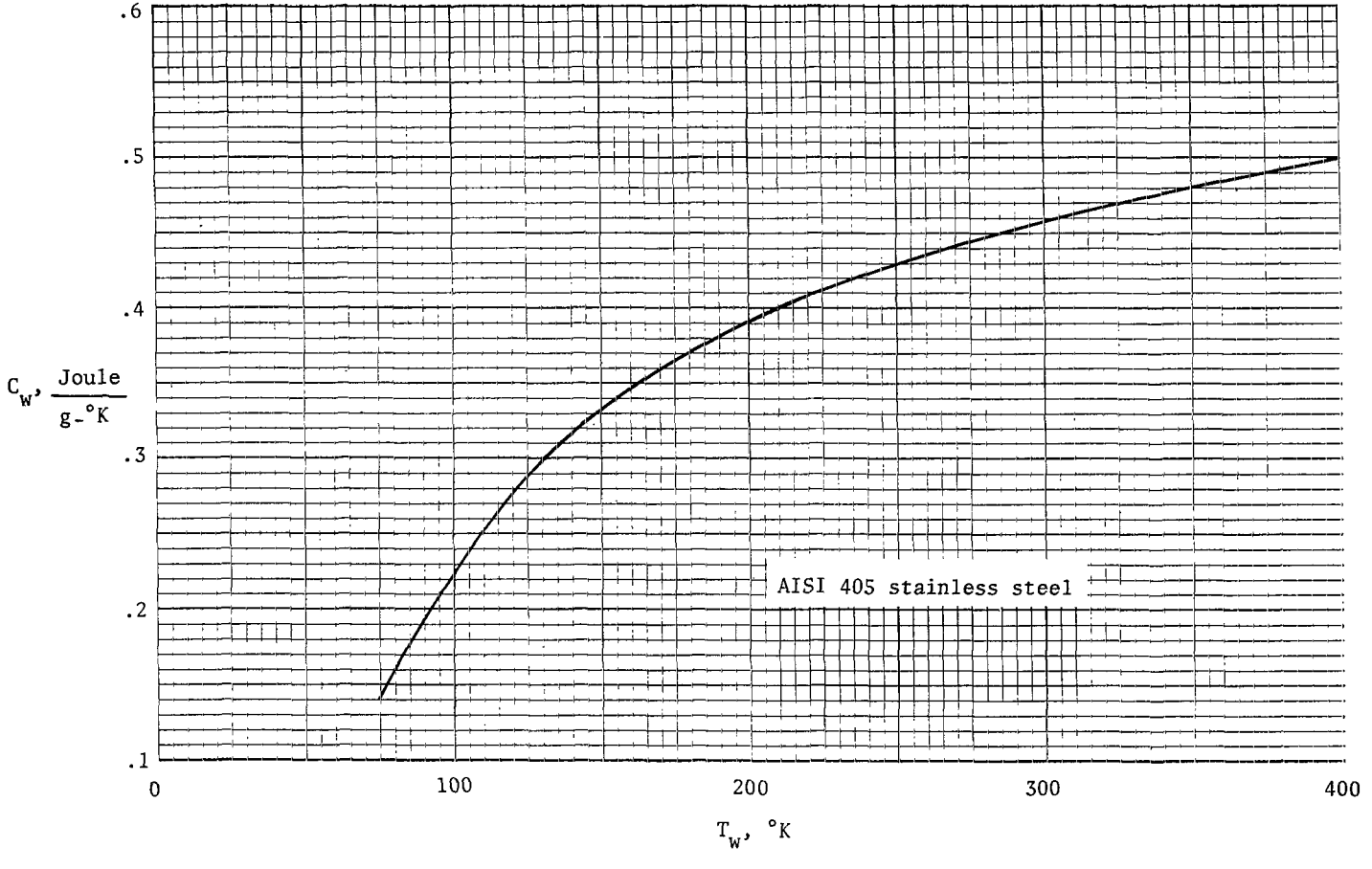

Figure 4.- Specific heat of model material.

Figure 5.- Schlieren showing flow details and model orientation. $M_e = 6.0$; $R_e/cm = 2.64 \times 10^5$. L-70-1622

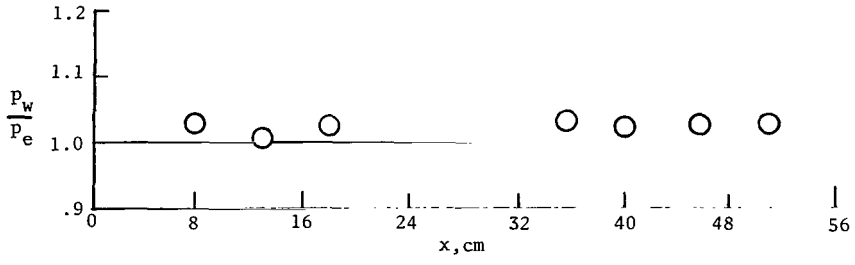

(a) $M_e = 6.0$; $T_w/T_t = 0.60$.

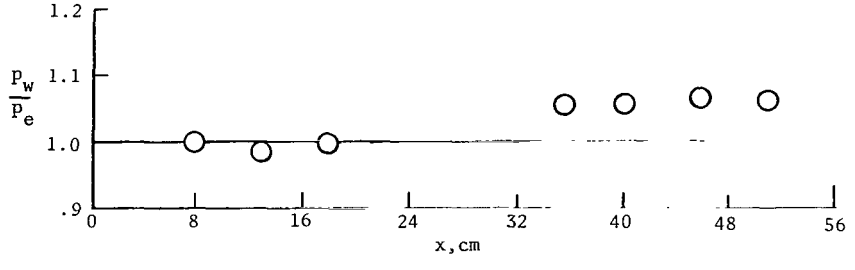

(b) $M_e = 6.0$; $T_w/T_t = 0.22$.

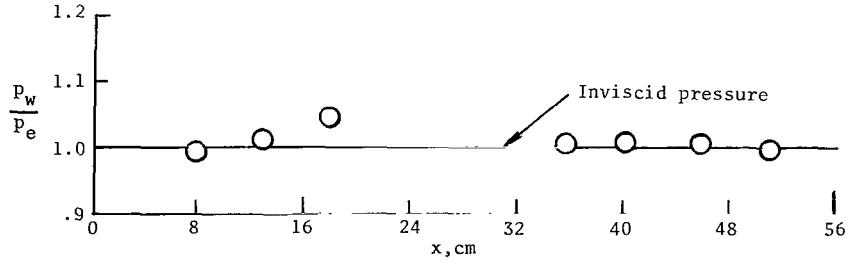

(c) $M_e = 4.9$; $T_w/T_t = 0.72$.

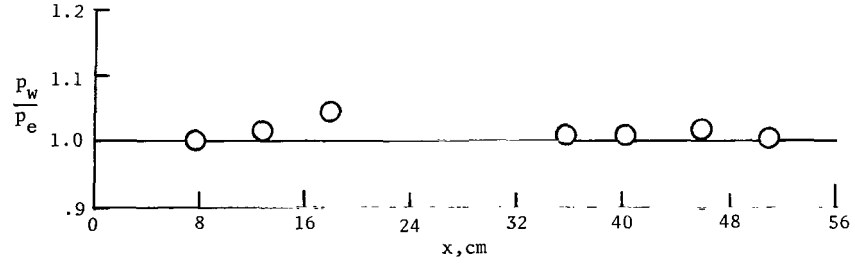

(d) $M_e = 4.9$; $T_w/T_t = 0.24$.

Figure 6.- Effect of wall cooling on surface pressure distribution. $R_\infty/cm = 2.64 \times 10^5$, $M_\infty = 6.0$.

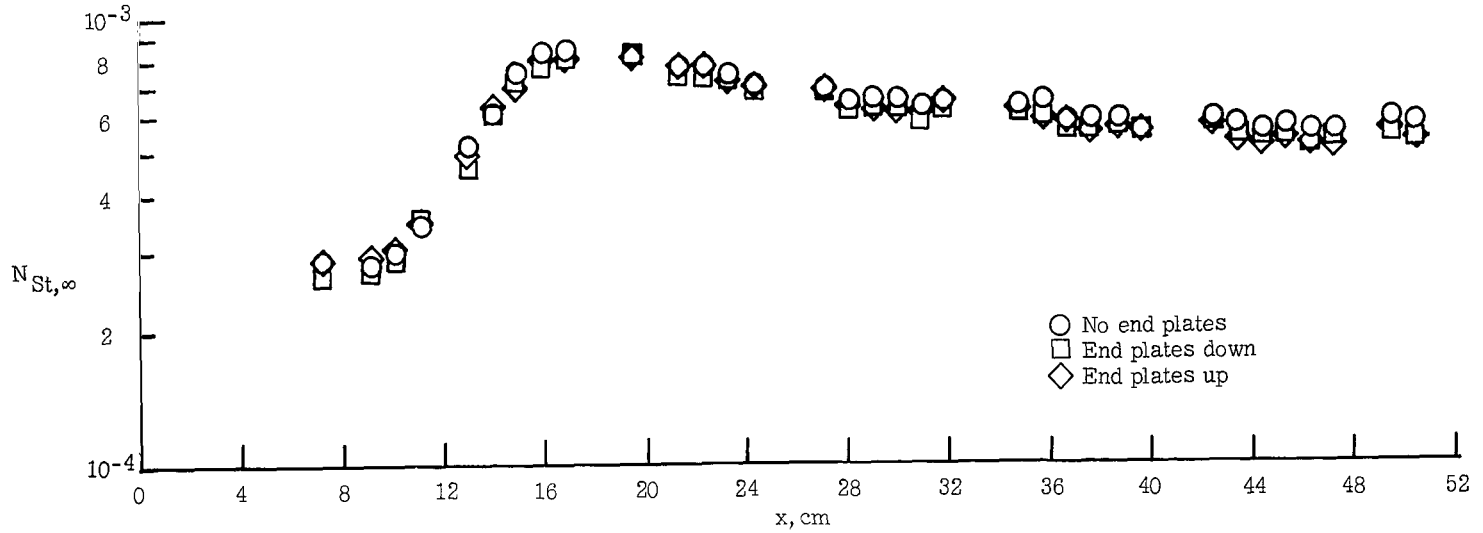

(a) $\alpha = 0^0$; $M_e = 6.0$; $R_e/cm = 0.264 \times 10^6$.

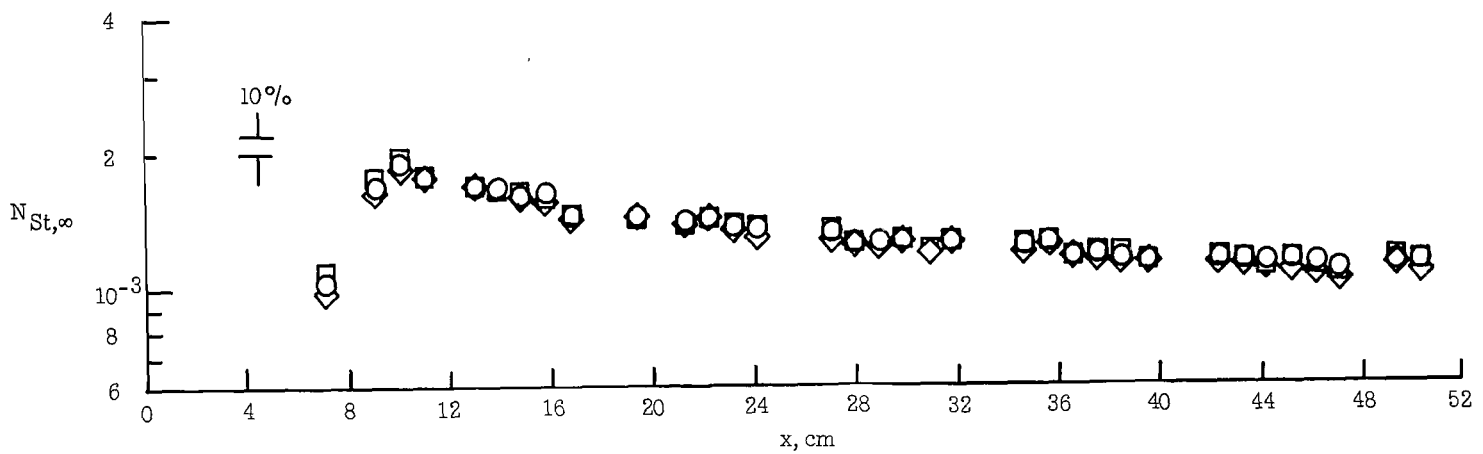

(b) $\alpha = 8.1^0$; $M_e = 4.9$; $R_e/cm = 0.378 \times 10^6$.

Figure 7.- Effect of end plate orientation on the surface heat transfer. $T_w/T_t = 0.60$.

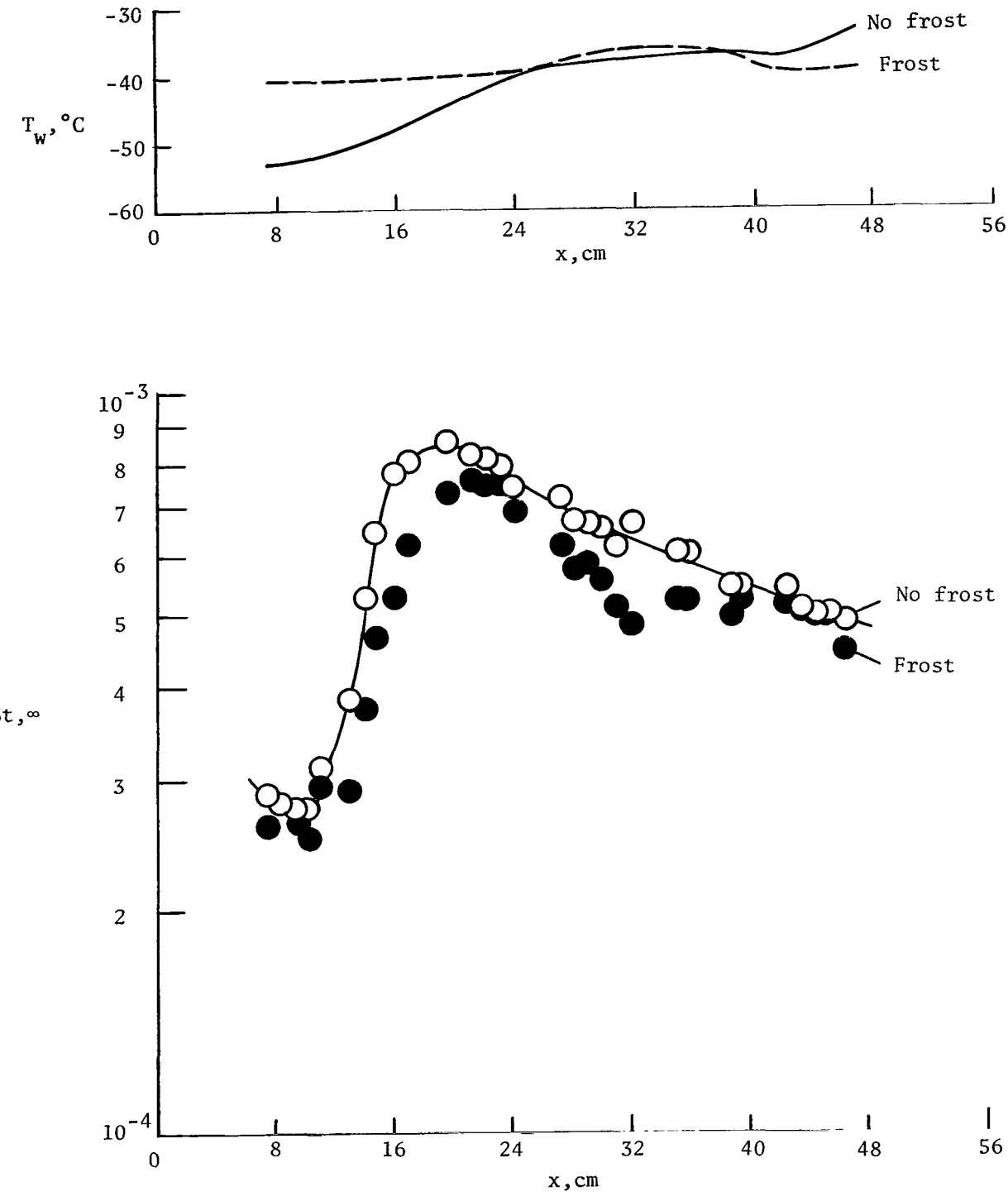

Figure 8.- Effect of surface frost on heat transfer and transition location. $\alpha = 0^0$; $M_e = 6.04$; $R_e/cm = 2.64 \times 10^5$.

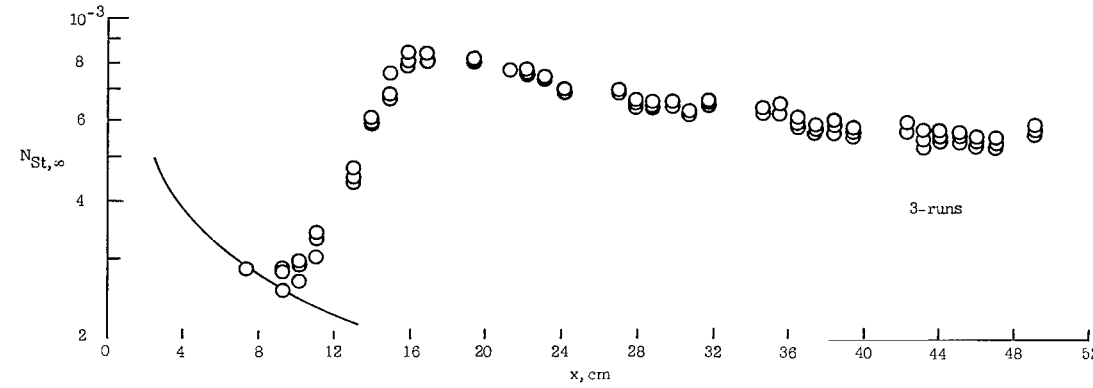

(a) $T_w/T_t = 0.6$.

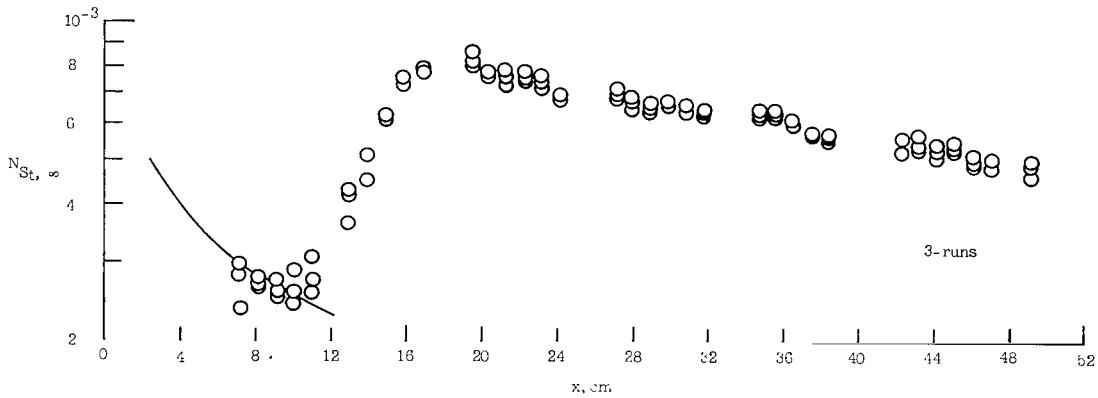

(b) $T_w/T_t = 0.4$.

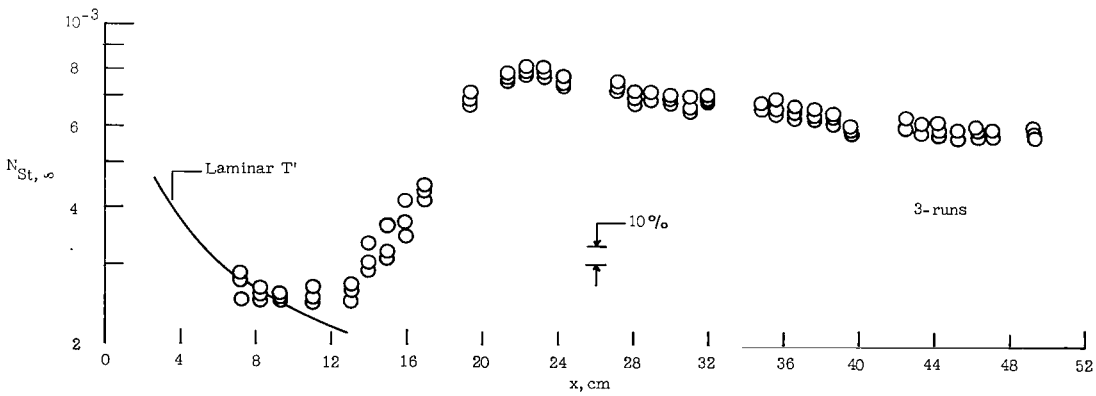

(c) $T_w/T_t = 0.2$.

Figure 9.- Heat-transfer distributions for various ratios of wall temperature to total temperature for $M_e = 6.0$; $\alpha = 0^o$; $R_e/cm = 2.64 \times 10^5$.

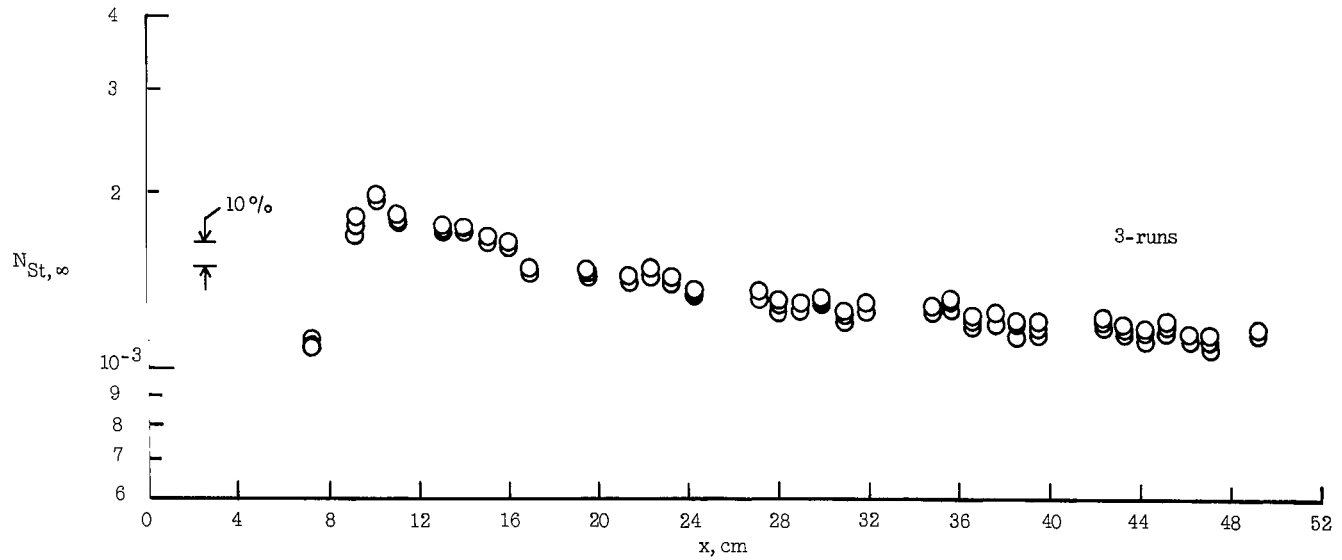

(a) $T_w/T_t = 0.6$.

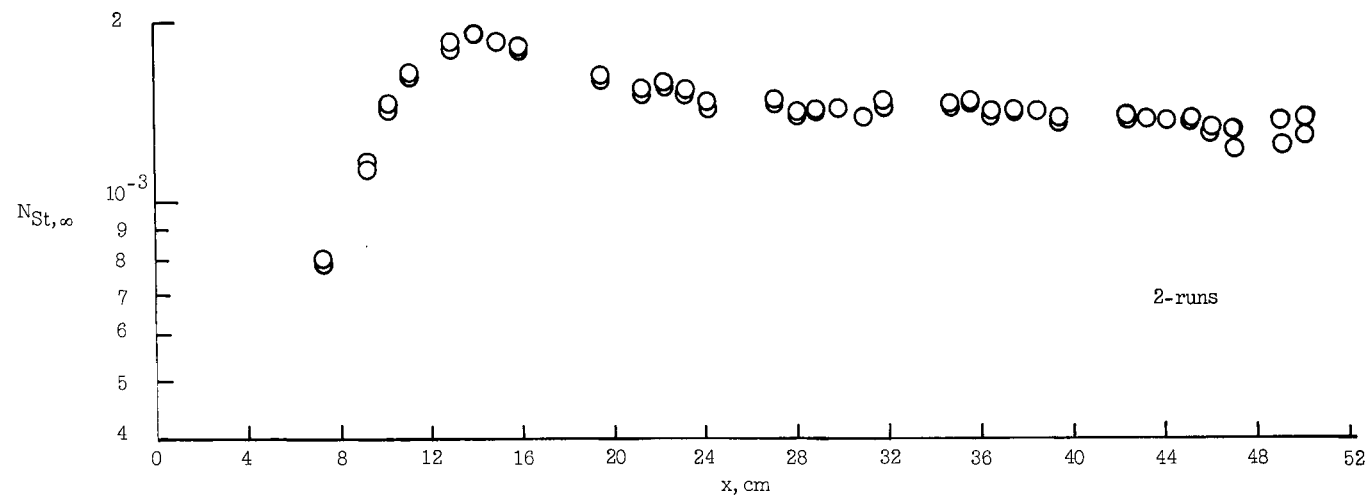

(b) $T_w/T_t = 0.3$.

Figure 10.- Heat-transfer distributions for various ratios of wall temperature to total temperature for $M_e = 4.9$; $\alpha = 8.1^0$; $R_e/cm = 3.78 \times 10^5$.

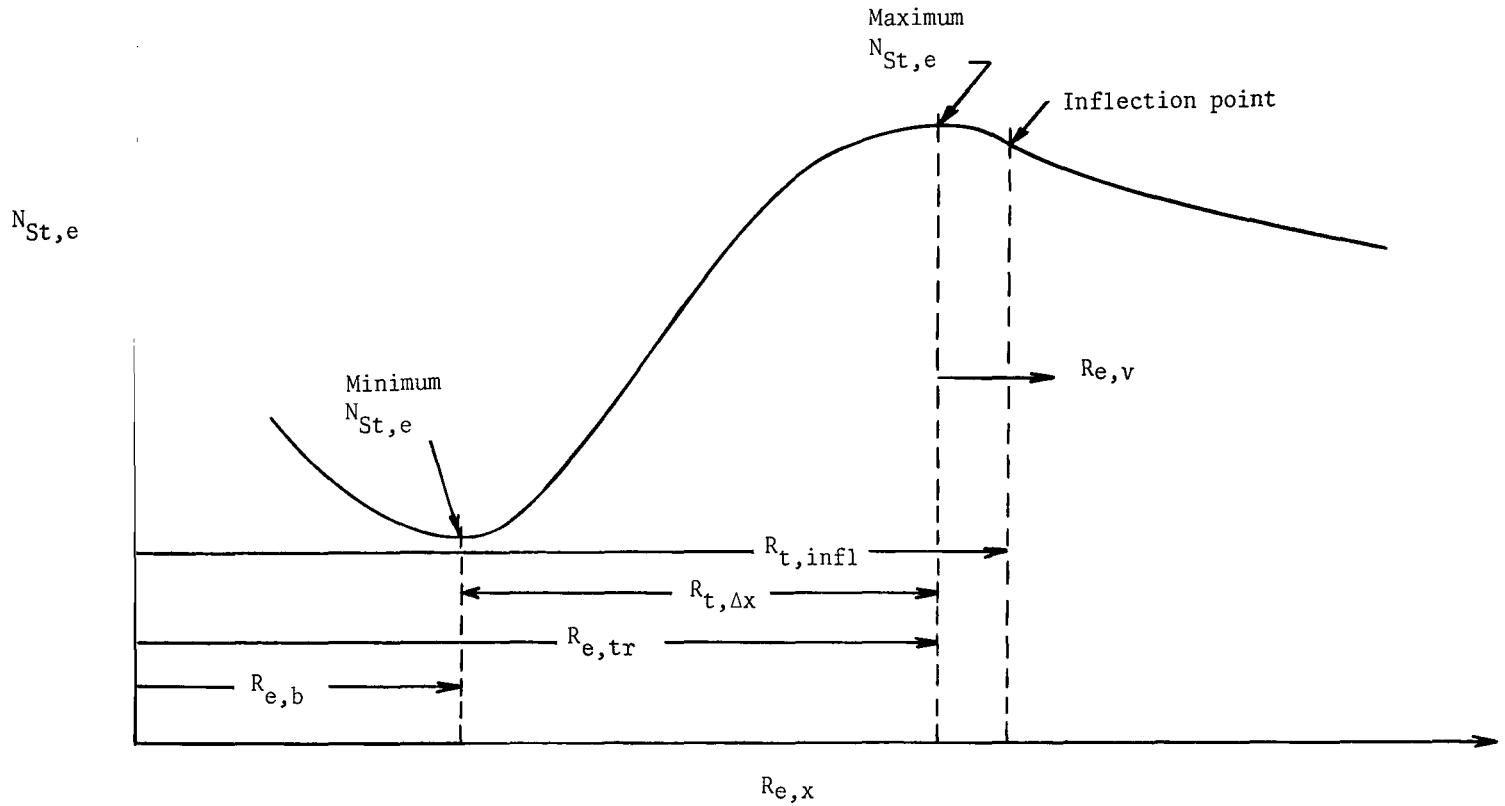

Figure 11.- Illustration of a typical heating distribution defining various length Reynolds numbers.

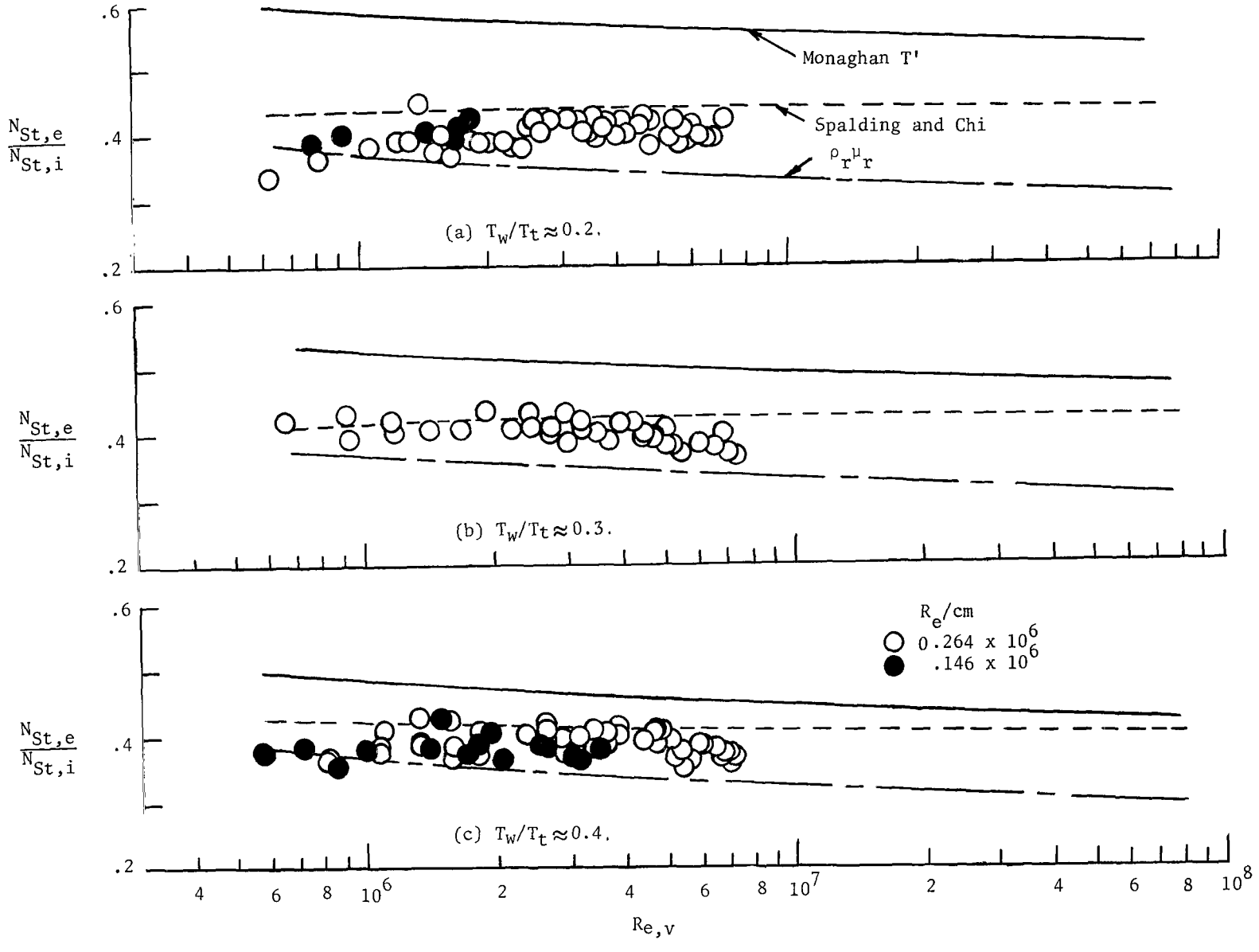

Figure 12.- Effect of local Reynolds number on turbulent heating for various wall temperature levels. M_e = 6.0.

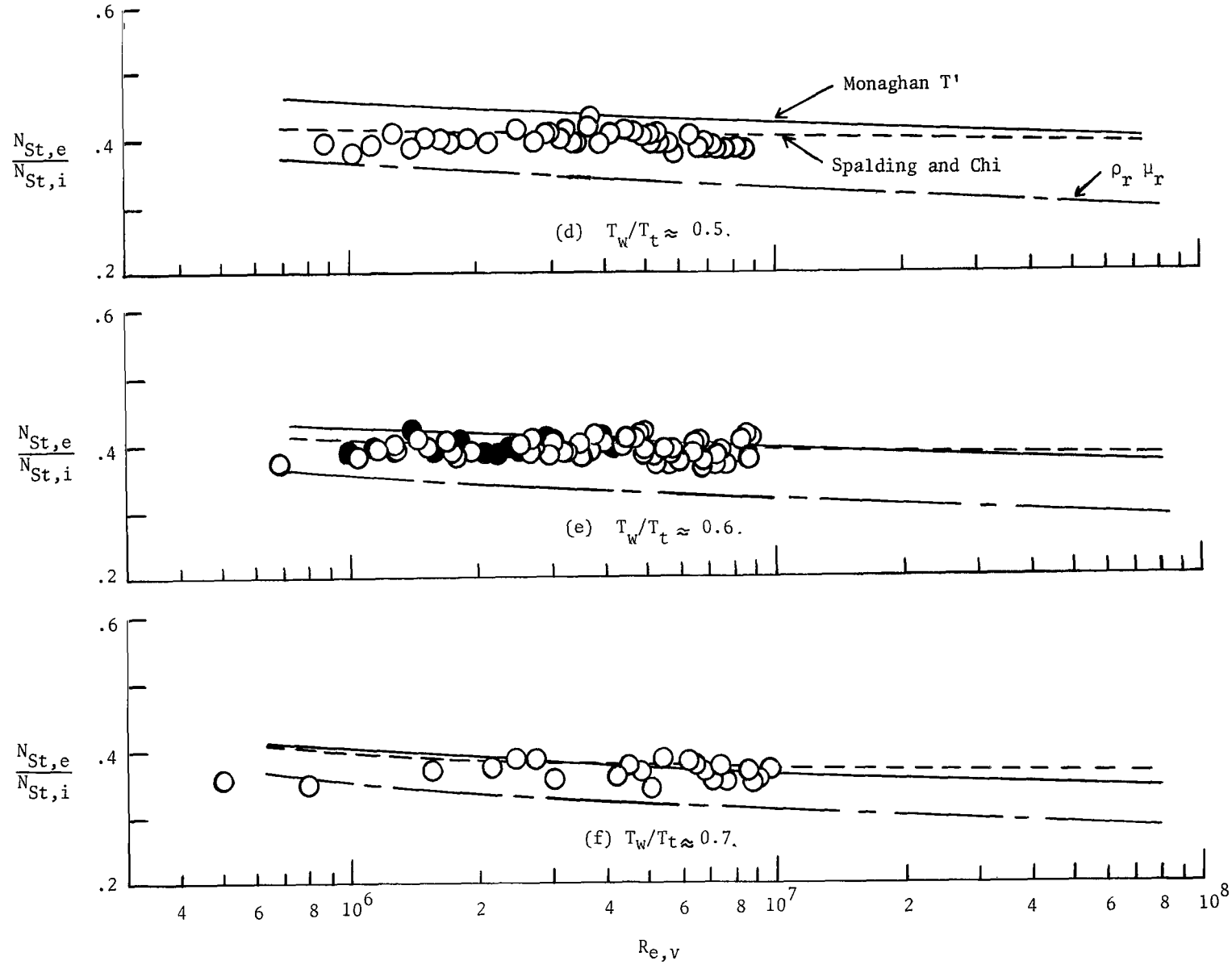

Figure 12.- Concluded.

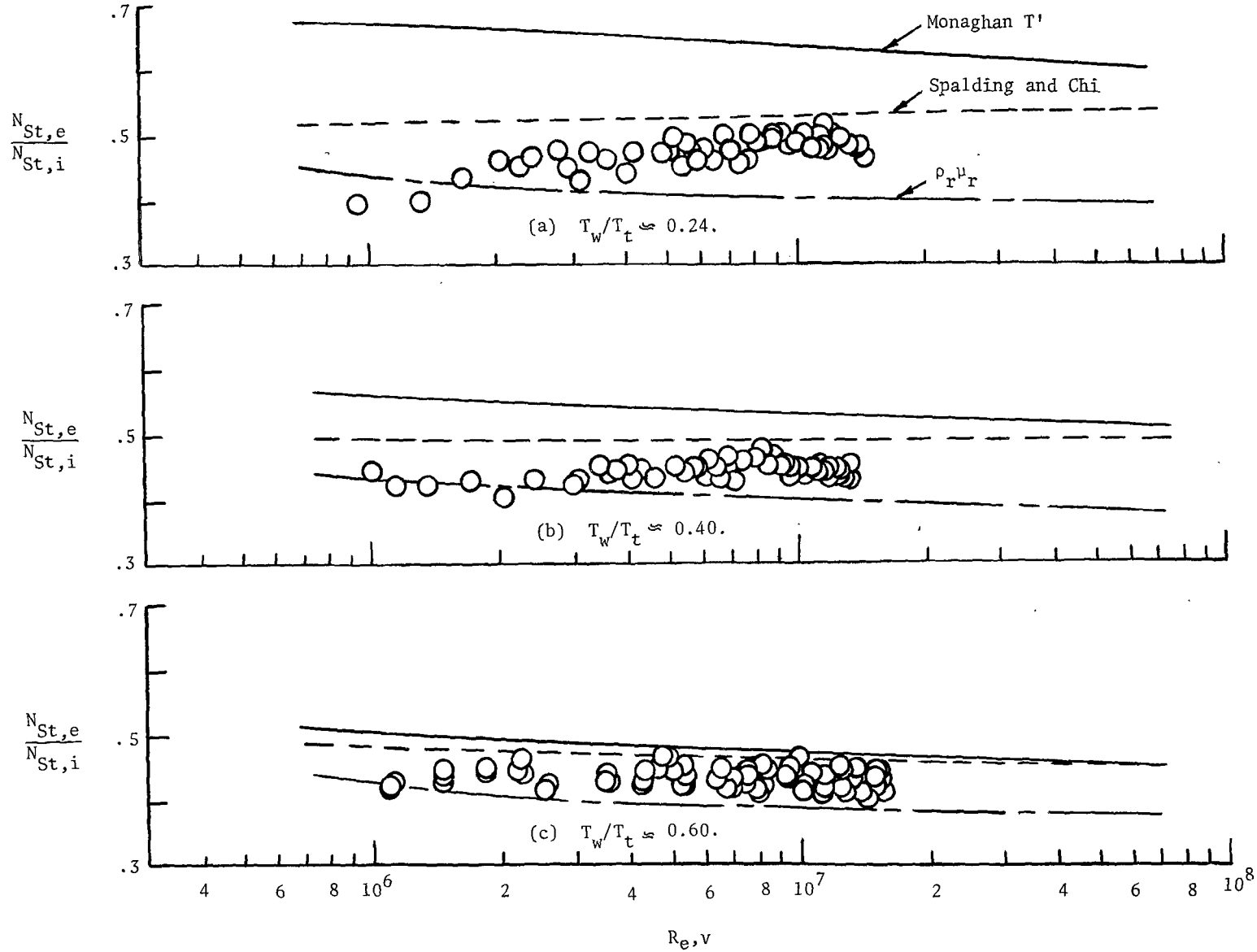

Figure 13.- Effect of local Reynolds number on turbulent heating for various wall temperature levels. $M_e = 4.9$; $R_e/cm = 3.82 \times 10^5$.

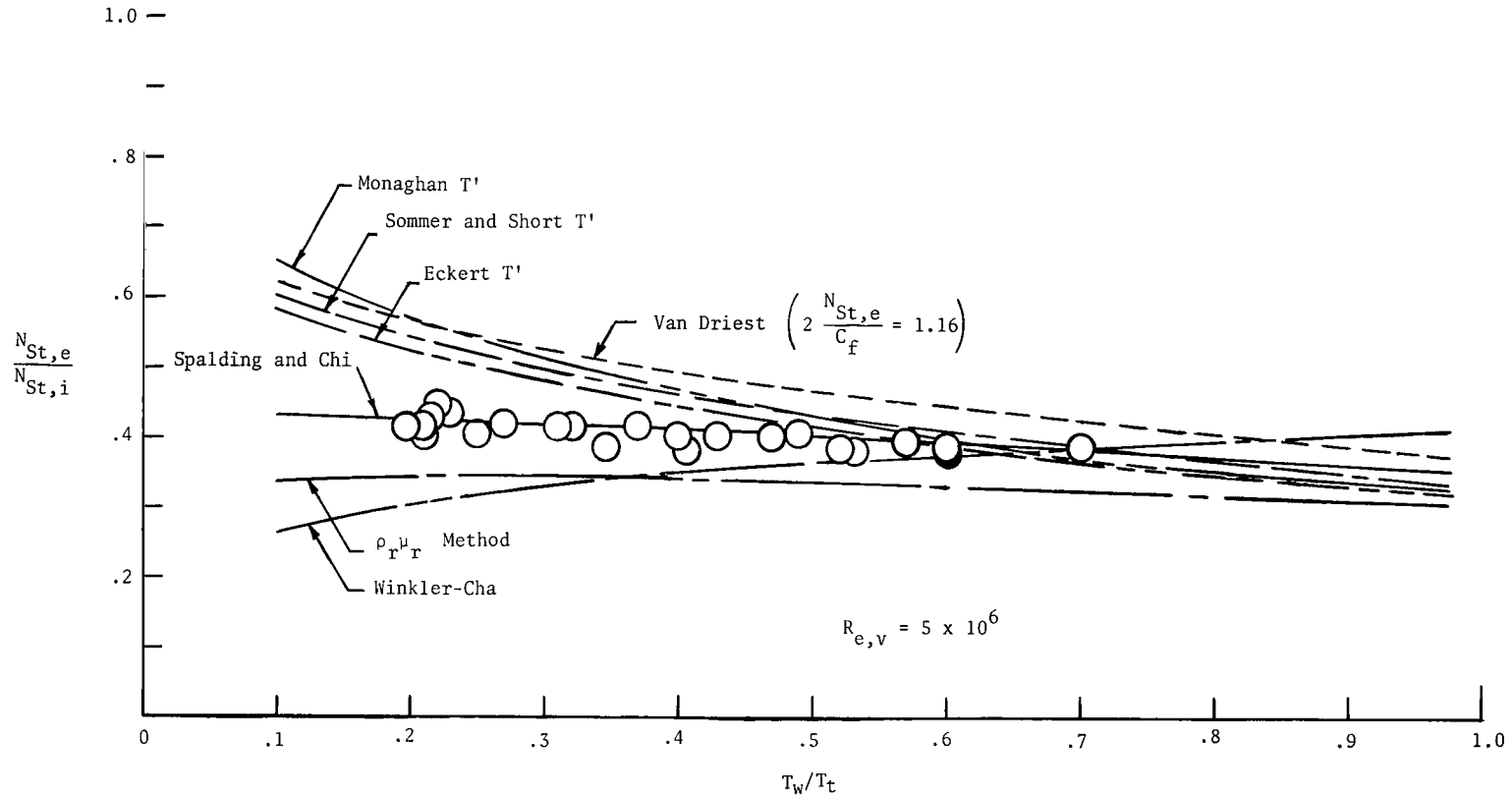

Figure 14.- Effect of wall cooling on turbulent boundary-layer heat transfer at $M_e = 6.0$; $\alpha = 0^0$.

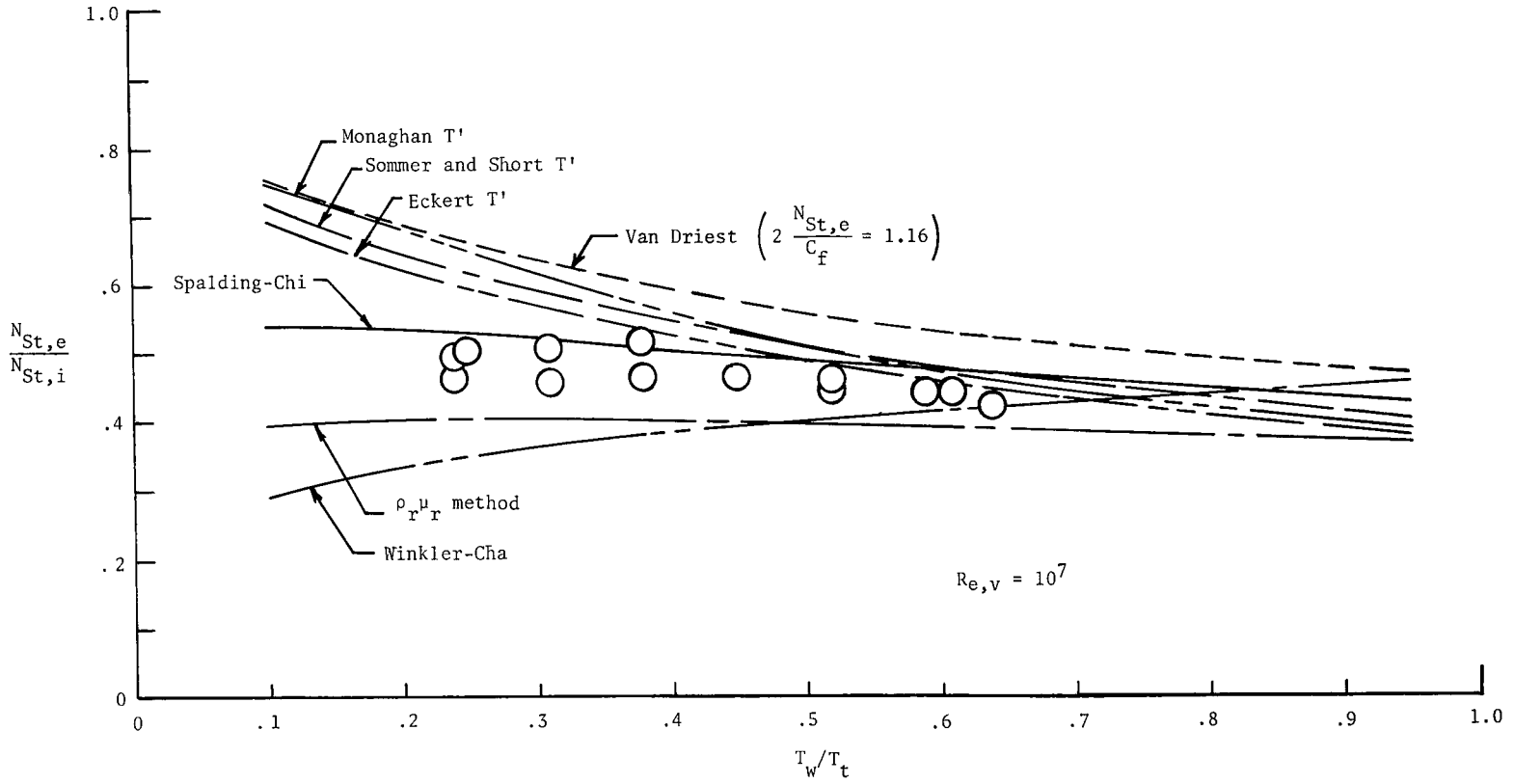

Figure 15.- Effect of wall cooling on turbulent heating at $M_e = 4.9$.

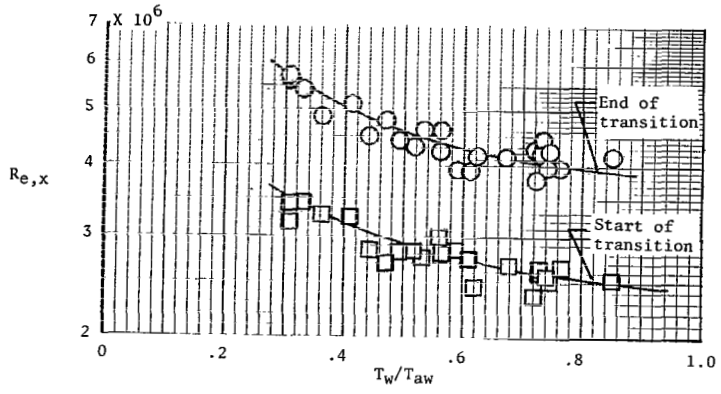

(a) $M_e = 6.0$; $R_e/cm = 2.64 \times 10^5$; $\alpha = 0^o$.

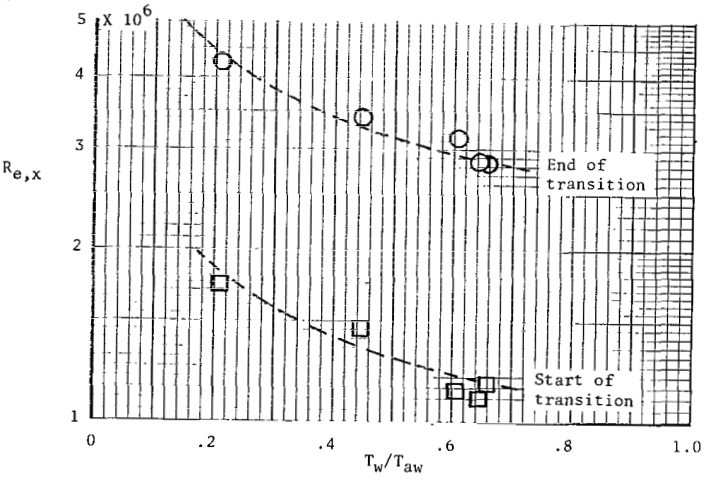

(b) $M_e = 6.0$; $R_e/cm = 1.46 \times 10^5$; $\alpha = 0^o$.

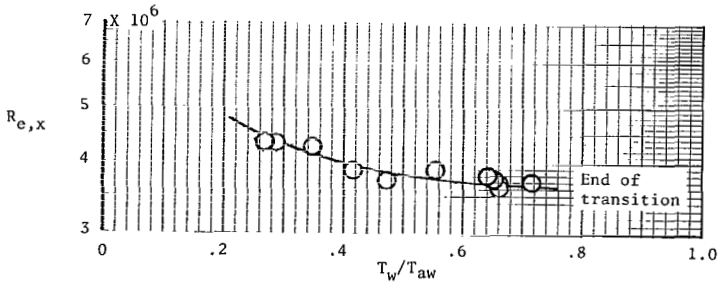

(c) $M_e = 4.9$; $R_e/cm = 3.82 \times 10^5$; $\alpha = 8.1^o$.

Figure 16.- Effect of wall cooling on the transition Reynolds number.

M_e	R_e/cm	Method to detect transition	Method to obtain T_w/T_{aw} variation	References
4.9	3.81×10^5	Heat transfer	Wall cooling	Present
6.0	1.46×10^5	Heat transfer	Wall cooling	Present
6.0	2.64×10^5	Heat transfer	Wall cooling	Present
2.4	0.98×10^5	Surface pitot	Wall heating	28
8.2	2.80×10^5	Schlieren	Wall cooling	15
8.2	2.48×10^5	Schlieren	Wall cooling	15,29
10.2	0.71×10^5	Surface pitot	Wall cooling	11
6.8	1.81×10^5	Heat transfer	Wall cooling	30 (Helium)
6.8	1.26×10^5	Heat transfer	Wall cooling	30 (Helium)

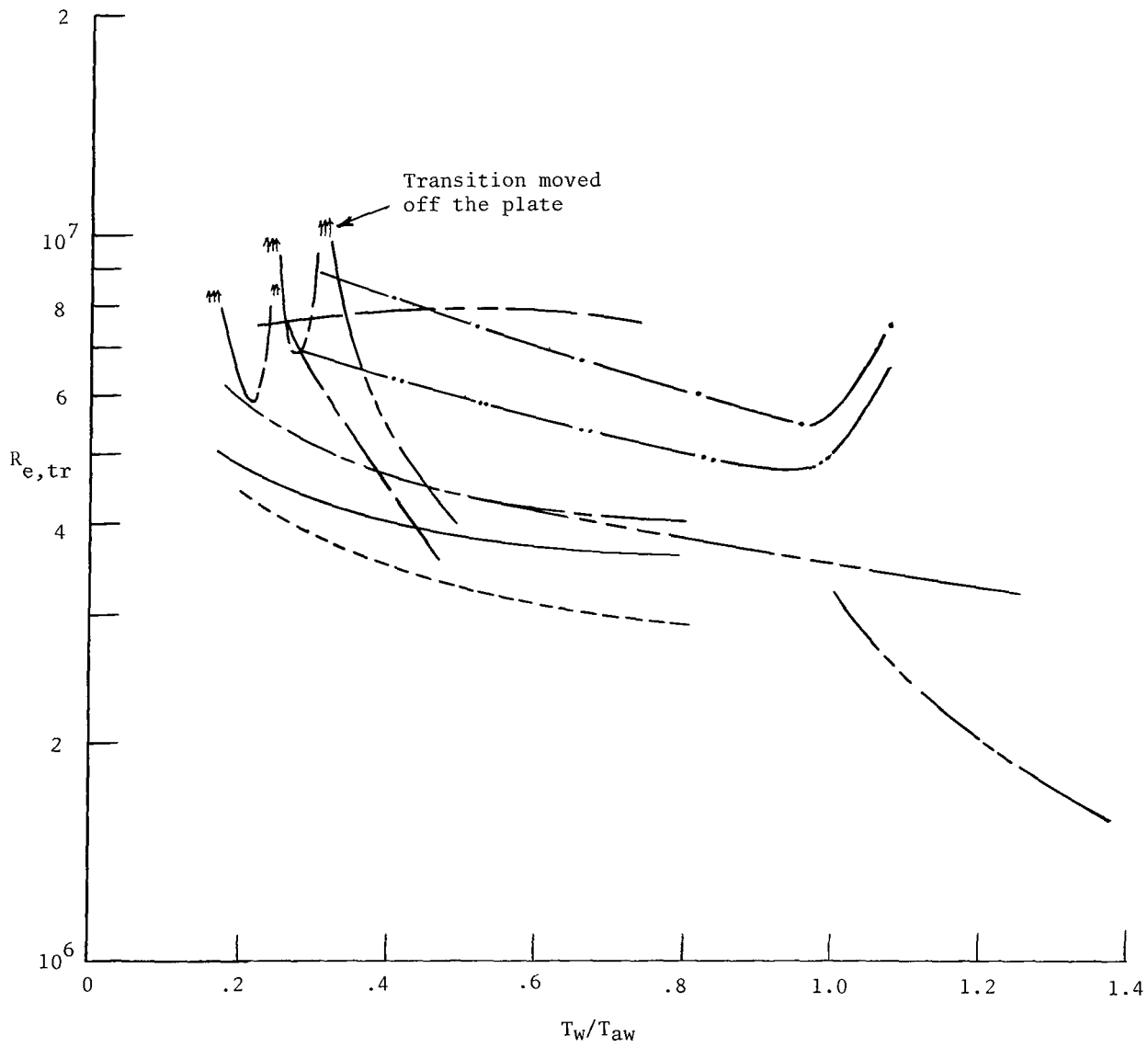

Figure 17.- Experimental transition results for flat plates with wall cooling.

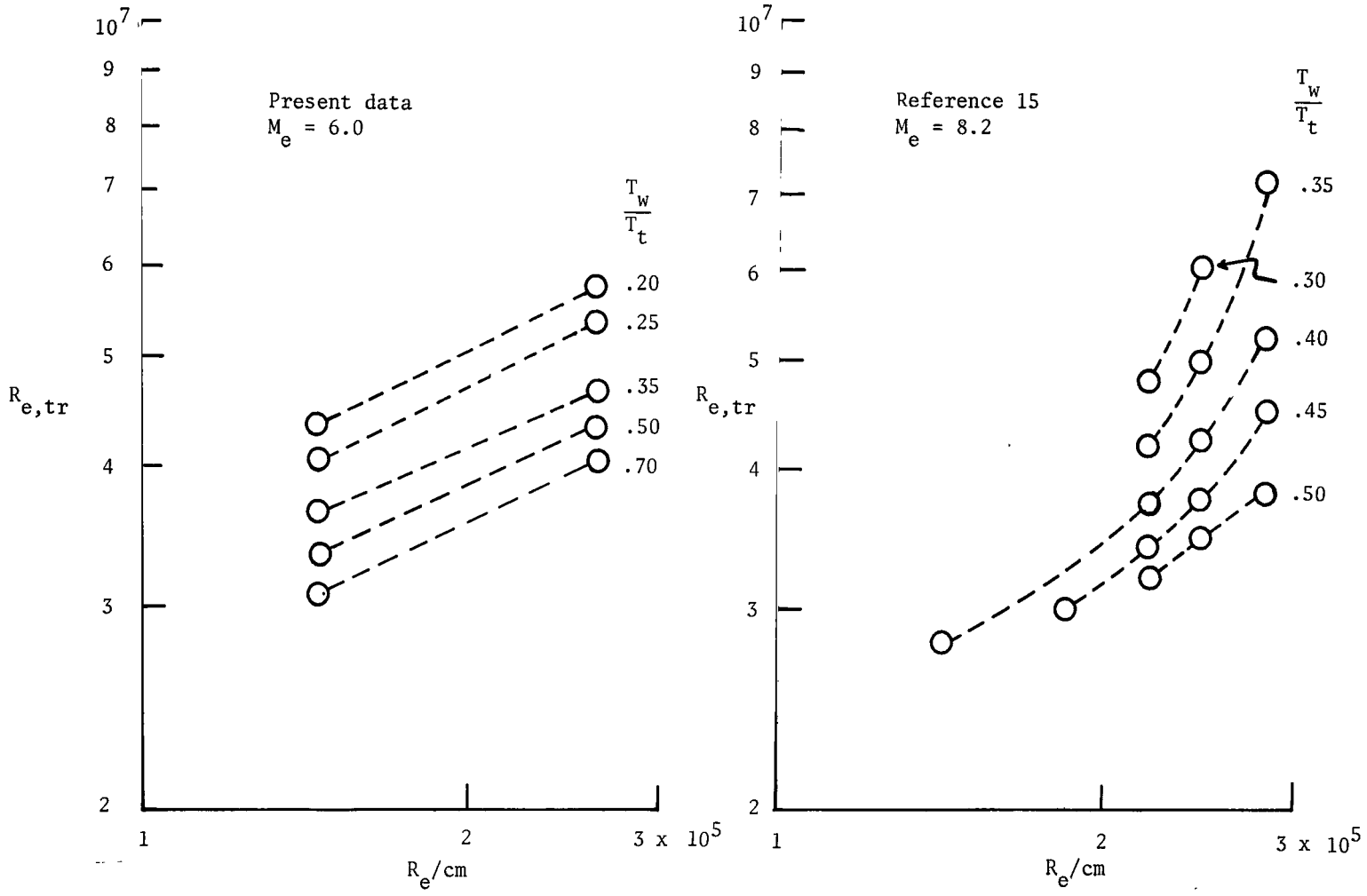

Figure 18.- Effect of unit Reynolds number on the transition Reynolds number for various wall temperature levels.

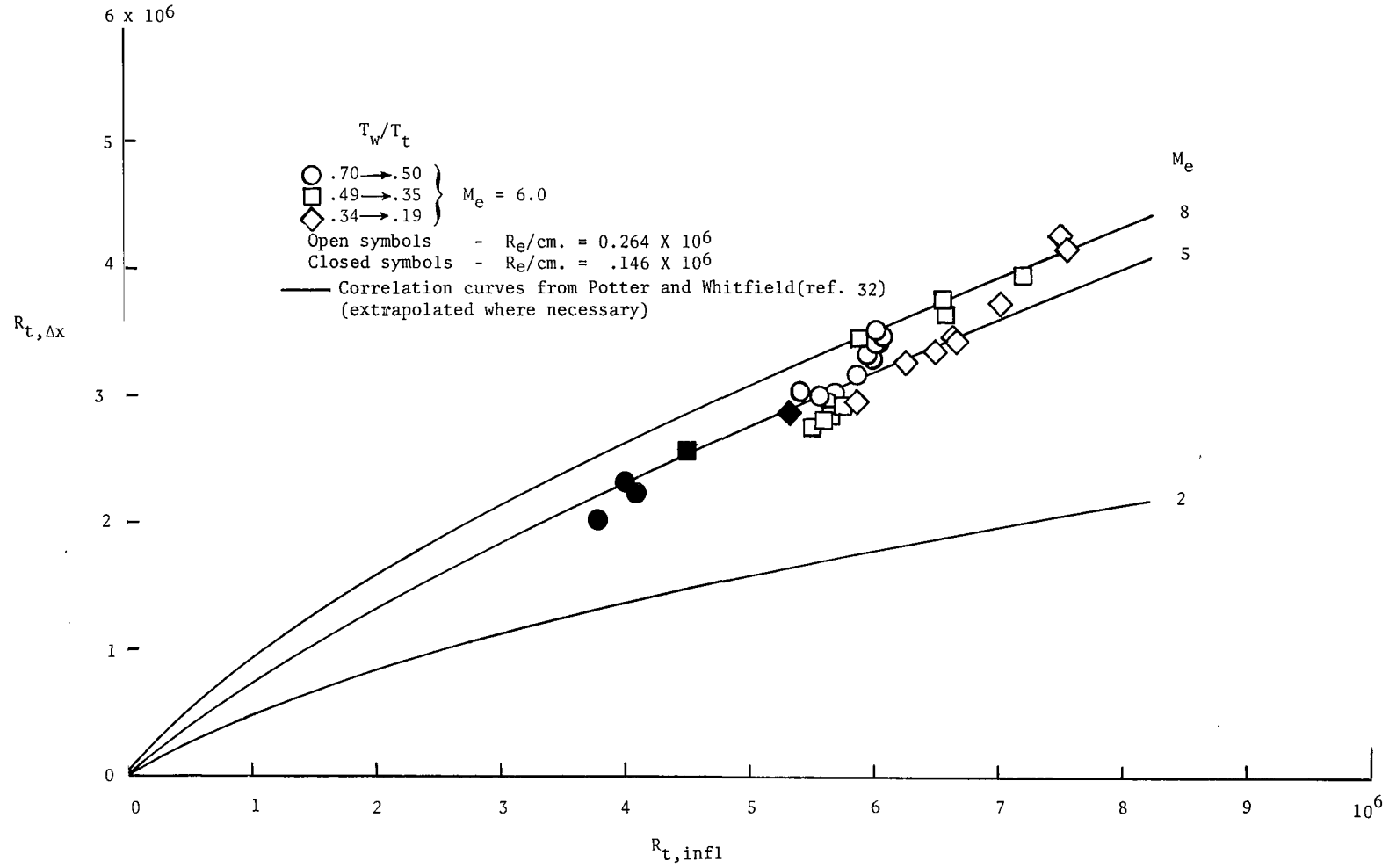

Figure 19.- Correlation of the Reynolds number based on the length of the transition region for various wall temperature levels.

NATIONAL AERONAUTICS AND SPACE ADMINISTRATION
WASHINGTON, D.C. 20546
OFFICIAL BUSINESS

FIRST CLASS MAIL

POSTAGE AND FEES PAID
NATIONAL AERONAUTICS AN
SPACE ADMINISTRATION

"The aeronautical and space activities of the United States shall be conducted so as to contribute . . . to the expansion of human knowledge of phenomena in the atmosphere and space. The Administration shall provide for the widest practicable and appropriate dissemination of information concerning its activities and the results thereof."

—NATIONAL AERONAUTICS AND SPACE ACT OF 1958

NASA SCIENTIFIC AND TECHNICAL PUBLICATIONS

TECHNICAL REPORTS: Scientific and technical information considered important, complete, and a lasting contribution to existing knowledge.

TECHNICAL NOTES: Information less broad in scope but nevertheless of importance as a contribution to existing knowledge.

TECHNICAL MEMORANDUMS: Information receiving limited distribution because of preliminary data, security classification, or other reasons.

CONTRACTOR REPORTS: Scientific and technical information generated under a NASA contract or grant and considered an important contribution to existing knowledge.

TECHNICAL TRANSLATIONS: Information published in a foreign language considered to merit NASA distribution in English.

SPECIAL PUBLICATIONS: Information derived from or of value to NASA activities. Publications include conference proceedings, monographs, data compilations, handbooks, sourcebooks, and special bibliographies.

TECHNOLOGY UTILIZATION PUBLICATIONS: Information on technology used by NASA that may be of particular interest in commercial and other non-aerospace applications. Publications include Tech Briefs, Technology Utilization Reports and Notes, and Technology Surveys.

Details on the availability of these publications may be obtained from:

SCIENTIFIC AND TECHNICAL INFORMATION DIVISION

NATIONAL AERONAUTICS AND SPACE ADMINISTRATION

Washington, D.C. 20546